Mixed-Valence Dialkylbiferrocenium Salts: An Explanation for the Observed Temperature Dependence of Electron-Transfer Rates

Teng-Yuan Dong,[1] David N. Hendrickson,*[1] Kumiko Iwai,[2] Michelle J. Cohn,[1] Steven J. Geib,[3] Arnold L. Rheingold,[3] Hirotoshi Sano,*[2] Izumi Motoyama,[2] and Satoru Nakashima[2]

Contribution from the School of Chemical Sciences, University of Illinois, Urbana, Illinois 61801, the Department of Chemistry, Faculty of Science, Tokyo Metropolitan University, Fukasawa, Setagaya-ku, Tokyo 158, Japan, and the Department of Chemistry, University of Delaware, Newark, Delaware 19716. Received June 6, 1985

Abstract: Data are presented to indicate that the rate of *intra*molecular electron transfer in mixed-valence biferrocenium triiodide, **1**, and four mixed-valence dialkyl-substituted biferrocenium triiodide salts is controlled by dynamics in the solid state. The X-ray structure of **1** at 296 K has been determined: $P\bar{1}$, a = 7.5779 (20) Å, b = 8.4742 (14) Å, c = 9.5577 (21) Å, α = 112.619 (14)°, β = 104.646 (20)°, and γ = 94.610 (19)°; Z = 1, D_{calcd} = 2.32 g cm^{-3}, R_{wF} = 0.042 for 2185 observed [$F_o \geq 2.5\sigma(F_o)$] reflections. The mixed-valence biferrocenium cation assumes a trans conformation where the Fe(η^5-C$_5$H$_5$) moieties are on opposite sides of a planar fulvenide ligand. The two rings bonded to each Fe atom are eclipsed. Both the cation and the anion sit on centers of symmetry in **1**. The 300 K Mössbauer spectrum of **1**, however, shows equal-area Fe^{II} and Fe^{III} doublets. It is probable that a well-formed single crystal has Mössbauer-delocalized molecules, whereas a microcrystalline sample tends to have localized molecules. Several different samples of **1** were examined with the Mössbauer technique to find that at 300 K the ratio of delocalized to localized molecules can vary from ~0 to ~1 depending on the history of the sample. At temperatures above 300 K the Mössbauer spectrum of compound **1** does change to eventually become a single average-valence doublet at ~357 K. Differential scanning calorimetry curves in the range of ~303 to ~363 K were run for several samples of **1**. For samples that show 300 K Mössbauer spectra comprised essentially of a localized signal, a relatively sharp endothermic peak is seen at ~335 K. Samples of **1** which show appreciable amounts of a signal for the delocalized species at 300 K give a broad DSC peak shifted to lower temperature than ~335 K. In one case the peak was apparently even so broad as to be not detectable. The X-ray structure of 1',6'-di-*n*-butylbiferrocenium triiodide, **7**, has been determined at 150, 298, and 363 K. At all three temperatures **7** crystallizes in the $P2_1/c$ space group. At 150 K the structure of **7** is characterized as a = 10.0201 (8) Å, b = 13.5203 (9) Å, c = 21.6080 (23) Å, and β = 106.015 (8)°; Z = 4, R_F = 0.042, and R_{wF} = 0.052 for 5145 observed ($|F|^2 > 2.0\sigma|F|^2$) reflections. The mixed-valence di-*n*-butylbiferrocenium cation assumes a trans conformation with a planar fulvenide ligand. The two halves of the cation are inequivalent at 150 K by virtue of the positioning of the I$_3^-$ anion and differences in the configuration of the two butyl groups. Analysis of the X-ray diffraction results for **7** at 298 and 363 K shows that at these higher temperatures positional disorder sets in for both the cation and the anion. One of the butyl groups develops pronounced positional disorder at the higher temperatures. It is suggested that this butyl group is dynamically disordered at the higher temperatures. This is supported by the observation that the c axis of a crystal of **7** expands appreciably from 150 to 363 K. Both **7** and 1',6'-dibenzylbiferrocenium triiodide, **8**, exhibit an interesting phenomenon. Microcrystalline samples of **7** and **8** give 300 K Mössbauer spectra which show appreciable intensity signals from valence-localized species, whereas recrystallized samples give 300 K Mössbauer spectra exhibiting only a signal for a delocalized species. At temperatures below ~200 K there are two doublets for crystalline **7** and **8**. The two doublets became a single doublet at ~275 and ~260 K, respectively, for **7** and **8** as the temperature is increased. The above results indicate that these mixed-valence compounds are undergoing phase transitions. It is suggested that the observed temperature dependence of the Mössbauer spectra for the dialkyl-substituted complexes **7** and **8** and the analogous ethyl- and propyl-substituted complexes results from I$_3^-$ anions undergoing a transformation from a static situation which tends to localize the charge in the mixed-valence cation to a dynamic situation where on the average the environment about each half of a mixed-valence cation is identical.

The fundamental nature of electron transfer between donor and acceptor sites that are separated by large distances is being studied. A variety of donor–linker–acceptor (DLA) molecules has been studied. In Dervan's[4] and others[5] DLA molecules the donor is a porphyrin, the acceptor is a quinone, and the linker is comprised of bicyclo[2.2.2]octane units. The steriodal 5α-androstane skeleton is the linker and various polyaromatics and quinoyl moieties serve as the donor and acceptor sites in Closs and Miller's studies.[6] In the work from the Gray,[7] Isied,[8] and Hoffman[9] groups a segment

of a protein serves as the linker and the donor and acceptor sites have transition-metal ions. Taube[10] and Cowan[11] pioneered the use of mixed-valence transition-metal complexes to probe electron transfer between well-separated metal sites. Various unsaturated and saturated organic linkers have been employed in these mixed-valence complexes.[12]

The focus of this and a later paper[13a] is electron transfer in the *solid state* for the following series of mixed-valence biferrocenium triiodide salts. Results for the compounds **2**, **3**, and **4** are discussed in a later paper,[13a] where with the aid of X-ray structural[13a,b] results

(1) University of Illinois.
(2) Tokyo Metropolitan University.
(3) University of Delaware.
(4) Joran, A. D.; Leland, B. A.; Geller, G. G.; Hopfield, J. J.; Dervan, P. B. *J. Am. Chem. Soc.* **1984**, *106*, 6091.
(5) Previous work listed in ref 4.
(6) Miller, J. R.; Calcaterra, L. T.; Closs, G. L. *J. Am. Chem. Soc.* **1984**, *106*, 3047.
(7) (a) Winkler, J. R.; Nocera, D. G.; Yocom, K. M.; Bordignon, E.; Gray, H. B. *J. Am. Chem. Soc.* **1982**, *104*, 5798. (b) Kostic, N. M.; Margalit, R.; Che, C.-M.; Gray, H. B. *Ibid.* **1983**, *105*, 7765.
(8) (a) Isied, S. S.; Worosila, G.; Atherton, S. J. *J. Am. Chem. Soc.* **1982**, *104*, 7659. (b) Isied, S. J. *Prog. Inorg. Chem.* **1984**, *32*, 443–517.
(9) Peterson-Kennedy, S. E.; McGourty, J. L.; Hoffman, B. M. *J. Am. Chem. Soc.* **1984**, *106*, 5010.
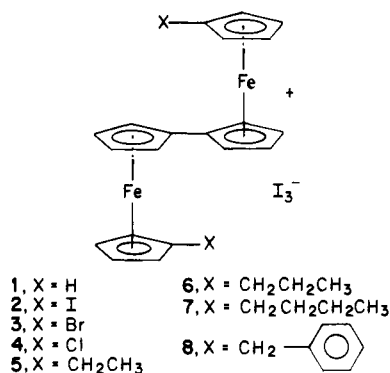
(10) Creutz, C.; Taube, H. *J. Am. Chem. Soc.* **1969**, *91*, 3988.
(11) Cowan, D. O.; Kaufman, F. *J. Am. Chem. Soc.* **1970**, *92*, 219.
(12) For recent reviews see: (a) Day, P. *Int. Rev. Phys. Chem.* **1981**,*1*, 149. (b) Brown, D. B., Ed. "Mixed-Valence Compounds, Theory and Applications in Chemistry, Physics, Geology and Biology"; Reidel Publishing Co.: Boston, 1980. (c) Creutz, C. *Prog. Inorg. Chem.* **1983**, *30*, 1–73. (d) Richardson, D. E.; Taube, H. *Coord. Chem. Rev.* **1984**, *60*, 107–129.
(13) (a) Dong, T.-Y.; Hendrickson, D. N.; Pierpont, C. G.; Moore, M. F. *J. Am. Chem. Soc.*, in press. (b) The results of the crystal structure of **2** have been communicated: Dong, T.-Y.; Cohn, M. J.; Hendrickson, D. N.; Pierpont, C. G. *J. Am. Chem. Soc.* **1985**, *107*, 4777–4778. (c) Cohn, M. J.; Dong, T.-Y.; Hendrickson, D. N.; Geib, S. J.; Rheingold, A. L. *J. Chem. Soc., Chem. Commun.* **1985**, 1095–1097.

the factors leading to slow ($<10^7$ s^{-1}) electron transfer in **4** and relatively fast ($>10^{10}$ s^{-1}) electron transfer in **2** and **3** are discussed. Compound **1** has been reported[14] to be localized on the Mössbauer time scale at 300 K. The X-ray crystal structure of **1** has very recently been reported.[13c] Compounds **5** and **6** each show one Fe^{II} and one Fe^{III} quadrupole-split doublet in Mössbauer spectra measured below 200 K. As the temperature of these compounds is increased above ~200 K the two doublets change to become eventually a *single average* quadrupole-split doublet at temperatures of 275 and 245 K, respectively.[15] In this paper are reported the preparation and characterization of the new compounds **7** and **8** as well as interesting observations on all of the complexes. Single-crystal X-ray structures are also reported for **1** and **7**. It is now known[13] that the mixed-valence cations in compounds **1**, **2**, **4**, **5**, **6**, and **7** have the trans conformation

1, X = H   6, X = CH$_2$CH$_2$CH$_3$
2, X = I   7, X = CH$_2$CH$_2$CH$_2$CH$_3$
3, X = Br
4, X = Cl   8, X = CH$_2$—⟨○⟩
5, X = CH$_2$CH$_3$

with Fe···Fe ≃ 5.1 Å (also probably the same for **3** and **8**). An explanation is advanced for the different observed temperature dependencies of electron-transfer rates in these compounds. In several cases a phase transition is suggested to explain the temperature dependence seen in the Mössbauer spectra. The conversion from "valence localized" at temperatures below ~200 K to "valence delocalized" at higher temperatures in several of these mixed-valence cations is facilitated by the onset of motion of the I$_3^-$ counterions.

Experimental Section

Compound Preparation. Samples of biferrocene[16] and 1',6'-dibenzylbiferrocene[17] were prepared according to literature methods and identified by melting point, NMR, and mass spectral data. 1',6'-Di-*n*-butylbiferrocene was prepared with the same synthetic approach employed for 1',6'-dibenzylbiferrocene. The properties of 1',6'-di-*n*-butylbiferrocene are the following: mp 52–53 °C; ^{1}H NMR (CDCl$_3$) δ 4.27 (4 H, t), 4.15 (4 H, t), 3.87 (8 H, s), 2.11 (4 H, t), 1.27 (8 H, m), 0.86 (6 H, t); electron-impact mass spectrum, M$^+$ at m/e 482.

Samples of 1',6'-di-*n*-butylbiferrocenium triiodide (**7**) and 1',6'-dibenyylbiferrocenium triiodide (**8**) were prepared according to the simple procedure previously reported for biferrocenium triiodide.[14] A microcrystalline compound results when a benzene solution of I$_2$ is slowly added to a benzene solution of the dialkylbiferrocene. In the case of **1**, **7**, and **8** crystals can be grown by the following diffusion experiment. The dialkylbiferrocenium triiodide salt is dissolved in CH$_2$Cl$_2$. Hexane is carefully added to form a separate layer above the CH$_2$Cl$_2$ solution. After a few days crystals form on the side of the container. Anal. Calcd for 1',6'-dibenzylbiferrocenium triiodide (**8**) (C$_{34}$H$_{30}$Fe$_2$I$_3$): C, 43.86; H, 3.25; I, 40.89. Found: C, 44.13; H, 3.14; I, 40.99. Calcd for 1',6'-di-*n*-butylbiferrocenium triiodide (C$_{28}$H$_{34}$Fe$_2$I$_3$): C, 38.97; H, 3.97; I, 44.11. Found: C, 38.71; H, 3.77; I, 44.32.

Physical Methods. At the University of Illinois ^{57}Fe Mössbauer measurements were made on a constant-acceleration-type instrument which has been described previously.[18,19] We estimate the absolute

(14) Morrison, W. H., Jr.; Hendrickson, D. N. *Inorg. Chem.* **1975**, *14*, 2331.

(15) Iijima, S.; Saida, R.; Motoyama, I.; Sano, H. *Bull. Chem. Soc. Jpn.* **1981**, *54*, 1375.

(16) Rausch, M. D. *J. Org. Chem.* **1961**, *26*, 1802.

(17) Yamakawa, K.; Hisatome, M.; Sako, Y.; Ichida, S. *J. Organomet. Chem.* **1975**, *93*, 219.

(18) Cohn, M. J.; Timken, M. D.; Hendrickson, D. N. *J. Am. Chem. Soc.* **1984**, *106*, 6683.

Table I. Experimental and Crystal Data for the X-ray Structure of Biferrocenium Triiodide at 296 K

Crystal Parameters

cryst syst: triclinic	space group: $P\bar{1}$
a = 7.5779 (20) Å	α = 112.619 (14)°
b = 8.4742 (14) Å	β = 104.646 (20)°
c = 9.5577 (21) Å	γ = 94.610 (19)°
V = 537.20 (19) Å^3	Z = 1
fw = 750.7	μ = 56.19 cm^{-1}
ρ(calcd) = 2.32 g cm^{-3}	ρ(obsd) = 2.3 g cm^{-3}

Data Measurement

diffractometer: Nicolet R3
radiation: graphite monochromatized Mo Kα
  (λ = 0.71069 Å)
2θ limits: 4.0° < 2θ < 55
data measured: 2435 ($\pm h,+k,+l$); data used:
  $F_o \geq 2.5\sigma(F_o)$ 2185 transmission
  (max/min): 0.585/0.372
$$R_F{}^a = 0.036; R_{wF}{}^a = 0.042$$

$^a R_F = \sum |F_o - |F_c||/\sum F_o$, $R_{wF} = [\sum w(F_o - |F_c|)^2/\sum wF_o^2]^{1/2}$.

Table II. Atom Coordinates ($\times 10^4$) and Thermal Factors (Å$^2 \times 10^3$) for Biferrocenium Triiodide

atom	x/a	y/b	z/c	$U_{iso}{}^a$
I(1)	0	0	0	51 (1)
I(2)	3634.2 (6)	771.3 (5)	2378.5 (5)	65 (1)
Fe(1)	-910.9 (8)	6298.5 (7)	2993.9 (7)	32 (1)
C(1)	453 (6)	5633 (5)	4795 (5)	35 (2)
C(2)	460 (6)	7452 (6)	5393 (5)	39 (2)
C(3)	1359 (6)	8177 (6)	4601 (5)	42 (2)
C(4)	1937 (6)	6822 (7)	3491 (5)	43 (2)
C(5)	1357 (6)	5248 (6)	3593 (5)	40 (2)
C(6)	-3582 (7)	6831 (9)	2634 (7)	60 (3)
C(7)	-3622 (9)	5026 (12)	2083 (11)	84 (4)
C(8)	-2737 (10)	4495 (7)	854 (7)	70 (3)
C(9)	-2146 (8)	6006 (7)	690 (6)	56 (2)
C(10)	-2676 (7)	7401 (7)	1771 (6)	52 (2)
H(2)	-32 (63)	7967 (60)	6166 (56)	31 (11)
H(3)	1340 (69)	9441 (62)	4755 (56)	43 (13)
H(4)	2536 (76)	6906 (69)	2797 (62)	54 (15)
H(5)	1718 (77)	4316 (76)	3088 (63)	46 (13)
H(6)	-3993 (104)	7585 (93)	3643 (83)	95 (23)
H(7)	-4022 (83)	4703 (78)	2397 (66)	40 (16)
H(8)	-2447 (135)	3200 (139)	381 (119)	147 (32)
H(9)	-1397 (88)	6226 (82)	-17 (75)	65 (17)
H(10)	-2393 (80)	8473 (74)	1888 (64)	59 (15)

$^a U_{iso}$ is the equivalent isotropic U defined as one-third of the trace of the orthogonalized U_{ij} tensor.

temperature accuracy to be ±3 K; the relative precision is ±0.5 K. Mössbauer spectra were least-squares fit to Lorentzian line shapes with a previously documented computer program.[20] An attempt was made to report isomer shift data relative to that of iron foil at 300 K; however, second-order Doppler effects could only be estimated due to source temperature variability (the source was located within the exchange-gas-cooled cryostat). It should be noted that the isomer shifts illustrated in the figures are plotted as experimentally obtained.

Infrared spectra were obtained with a Nicolet Model MX-5 FT spectrometer. All samples were prepared as 13-mm KBr pellets with 2–5 mg of compound mixed well with 150 mg of KBr. A Spectrim closed-cycle refrigerator (Cryogenic Technology, Inc.) was used to cool the KBr pellets to ~50 K. The temperature of the KBr-pellet holder was monitored with an iron-doped gold vs. chromel thermocouple.

X-ray Structure Solution and Refinement for Biferrocenium Triiodide (1). A block-like crystal (0.18 × 0.20 × 0.36 mm) of **1** grown by the CH$_2$Cl$_2$/hexane diffusion technique was used for data collection at 296 K on a Nicolet R3 automated diffractometer at the University of Delaware. Details of data collection may be found in Table I. No evidence for crystal decomposition was noted. The unit cell parameters, listed in Table I, were obtained by a least-squares fit to the automatically centered settings for 25 reflections. The data were corrected for Lorentz, polar-

(19) Federer, W. D. Ph.D. Thesis, University of Illinois, 1984.

(20) Chrisman, B. L.; Tumolillo, T. A. *Comput. Phys. Commun.* **1971**, *2*, 322.

Table III. Experimental and Crystal Data for the X-ray Structure of Di-*n*-butylbiferrocenium Triiodide at 150 K

Crystal Parameters

cryst syst: monoclinic	space group $P2_1/c$
$a = 10.0201$ (8) Å	$\alpha = 90°$
$b = 13.5203$ (9) Å	$\beta = 106.015$ (8)°
$c = 21.6080$ (23) Å	$\gamma = 90°$
$V = 2813.7$ (4) Å^3	$Z = 4$
fw = 862.92	ρ(calcd) = 2.045 g cm^{-3}

Data Measurement

radiation: graphite monochromatized Mo
$K\alpha$ ($\lambda = 0.7106$ Å)
2θ limit: $2\theta < 58.0°$
data measd: 7478 ($\pm h, +k, +l$); data used:
$|F_o|^2 > 2.0\sigma|F_o|^2$ 5145
$R_F{}^a = 0.042$; $R_{wF}{}^a = 0.052$

$^a R_F = \sum||F_o| - |F_c||/\sum|F_o|$, $R_{wF} = [\sum w(F_o - |F_c|)^2/\sum wF_o^2]^{1/2}$.

ization, and anomalous dispersion effects. The data were also corrected for absorption.

The structure of **1** was solved by intuitively placing an I atom at 0,0,0. The remaining non-hydrogen atoms were located by a series of difference Fourier syntheses. All non-hydrogen atoms were refined with anisotropic thermal parameters. All hydrogen atoms were located and isotropically refined. The final positional parameters for all atoms can be found in Table II. Listings of the anisotropic thermal parameters and observed and calculated structure factors are given in the supplementary material.

X-ray Structure Solution and Refinement for 1′,6′-Di-*n*-butylbiferrocenium Triiodide (7). Black needle crystals, which were grown by slow evaporation from a CH_2Cl_2 solution, were sealed in Lindemann glass capillaries filled with N_2 gas. It was found that when these crystals are exposed to air they suffer some decomposition over a period of time. Preliminary oscillation and Weissenberg photographs were taken at room temperature by using Cu $K\alpha$ radiation. The crystal was determined to be monoclinic. X-ray diffraction data were collected at 150, 298, and 363 K. The space group was confirmed to be $P2_1/c$ at all three temperatures. The final unit cell dimensions were refined by the least-squares method based on 16 reflections at 150 K, 25 reflections at 298 K, and 16 reflections at 363 K.

The equipment used to cool the crystal of **7** was constructed of stainless steel according to the description of Bolhuis.[21] Crystal specimens were cooled by a stream of cold N_2 gas which was surrounded by a warmer stream of N_2 gas. The temperature was maintained at 150 ± 1 K throughout the data collection by careful monitoring with a thermocouple. The high-temperature apparatus consisted of a heater mounted on a stainless steel tube. The temperature control at 363 K was effected with a precision of ±0.25 °C.

A periodic check of three and four standard reflections at 150 and 298 K, respectively, observed every 50 reflections, showed that there was slow crystal decomposition during data collection. Intensity data were corrected for this slow decomposition. At 363 K crystals decomposed on storing over a period of several days. Several crystals of approximate dimensions 0.30 × 0.30 × 0.30 mm cut from the same crystal were employed for data collection. Intensity corrections were carried out with the intensities of three standard reflections.

The 150 K X-ray structure of **7** was solved by the conventional heavy-atom method. Details of data collection and unit cell parameters are given in Table III. The positions of Fe and I atoms were deduced from sharpened Patterson maps. Successive three-dimensional Fourier synthesis phased by these atoms yielded the positions of all C atoms. Difference Fourier maps clarified the positions of H atoms. Anisotropic thermal parameters were used for non-hydrogen atoms and isotropic thermal parameters for the hydrogen atoms. The final positional parameters for all atoms can be found in Table IV. Listings of the thermal parameters and observed and calculated structure factors are given in the supplementary material. Atomic scattering factors for non-hydrogen atoms were taken from "International Tables for X-ray Crystallography",[22] and those for H atoms were from Stewart et al.[23] Unit weights were adopted for all reflections.

Although the solution and refinement of the 298 K structure of **7** are similar to those described above for the 150 K data set, the positions of the hydrogen atoms could not be determined. The unit cell parameters

Table IV. Atom Coordinates (×10^5 for I and Fe; ×10^4 for C; ×10^3 for H) and Thermal Parameters (Å^2 × 10) for Di-*n*-butylbiferrocenium Triiodide at 150 K

atom	x/a	y/b	z/c	B_{eq}
I(1)	24440 (7)	7580 (4)	8277 (3)	245 (2)
I(2)	23639 (5)	7320 (4)	21579 (3)	166 (1)
I(3)	23819 (6)	6631 (4)	35199 (3)	200 (1)
Fe(1)	26325 (11)	42597 (8)	33823 (5)	106 (2)
Fe(2)	25811 (11)	71463 (8)	18334 (5)	106 (2)
C(1)	3808 (8)	4612 (6)	2754 (4)	14 (2)
C(2)	3379 (8)	3593 (6)	2683 (4)	15 (2)
C(3)	1883 (8)	3589 (6)	2495 (4)	15 (2)
C(4)	1402 (8)	4587 (6)	2452 (4)	13 (2)
C(5)	2602 (8)	5222 (5)	2594 (3)	11 (2)
C(6)	3899 (8)	4408 (6)	4321 (4)	16 (2)
C(7)	3381 (9)	3423 (6)	4206 (4)	17 (2)
C(8)	1873 (9)	3476 (6)	4032 (4)	18 (2)
C(9)	1490 (9)	4500 (6)	4056 (4)	16 (2)
C(10)	2755 (9)	5076 (6)	4244 (4)	14 (2)
C(11)	2876 (9)	6180 (6)	4327 (4)	18 (2)
C(12)	1486 (9)	6716 (6)	4183 (4)	14 (2)
C(13)	1674 (9)	7833 (6)	4249 (4)	19 (2)
C(14)	314 (9)	8368 (7)	4180 (4)	22 (2)
C(1′)	3757 (8)	6941 (6)	2765 (4)	15 (2)
C(2′)	3269 (9)	7935 (6)	2686 (4)	16 (2)
C(3′)	1766 (9)	7912 (6)	2473 (4)	16 (2)
C(4′)	1329 (8)	6902 (6)	2425 (4)	15 (2)
C(5′)	2566 (8)	6288 (5)	2616 (4)	12 (2)
C(6′)	3826 (8)	6932 (6)	1221 (4)	14 (2)
C(7′)	3232 (9)	7910 (6)	1150 (4)	18 (2)
C(8′)	1730 (8)	7796 (6)	956 (4)	16 (2)
C(9′)	1435 (8)	6762 (6)	922 (4)	15 (2)
C(10′)	2712 (9)	6233 (6)	1083 (4)	16 (2)
C(11′)	2922 (10)	5129 (6)	1075 (4)	19 (2)
C(12′)	2632 (10)	4733 (6)	389 (4)	20 (2)
C(13′)	3013 (10)	3629 (6)	372 (4)	20 (2)
C(14′)	4545 (11)	3447 (8)	498 (5)	32 (3)
H(1)	480 (7)	484 (5)	290 (3)	2 (17)
H(2)	421 (11)	294 (8)	283 (5)	47 (32)
H(3)	119 (10)	303 (7)	238 (4)	27 (25)
H(4)	43 (8)	484 (6)	232 (4)	13 (21)
H(6)	490 (8)	461 (6)	447 (4)	10 (20)
H(7)	403 (10)	281 (7)	425 (4)	29 (26)
H(8)	95 (11)	289 (8)	381 (5)	46 (32)
H(9)	38 (9)	479 (7)	396 (4)	25 (25)
H(11A)	476 (9)	673 (6)	294 (4)	15 (22)
H(11B)	417 (14)	854 (11)	291 (6)	83 (46)
H(12A)	82 (14)	868 (10)	237 (6)	79 (45)
H(12B)	23 (10)	666 (7)	223 (4)	30 (26)
H(13A)	487 (8)	674 (6)	140 (4)	6 (19)
H(13B)	401 (11)	853 (8)	131 (5)	40 (30)
H(14A)	84 (11)	835 (8)	84 (5)	41 (30)
H(14B)	43 (10)	650 (7)	79 (4)	26 (25)
H(14C)	371 (10)	625 (7)	485 (4)	27 (25)
H(1′)	373 (10)	640 (8)	410 (5)	37 (28)
H(2′)	59 (14)	633 (10)	448 (6)	74 (42)
H(3′)	66 (10)	649 (7)	376 (4)	25 (25)
H(4′)	220 (13)	807 (10)	460 (6)	66 (40)
H(6′)	171 (14)	825 (10)	394 (6)	75 (42)
H(7′)	−1 (11)	816 (8)	457 (5)	37 (29)
H(8′)	−34 (8)	818 (6)	380 (4)	13 (21)
H(9′)	32 (11)	910 (8)	419 (5)	46 (32)
H(11′A)	228 (12)	493 (9)	122 (6)	60 (37)
H(11′B)	413 (11)	507 (8)	132 (5)	40 (29)
H(12′A)	123 (13)	489 (10)	12 (6)	71 (41)
H(12′B)	381 (14)	527 (10)	32 (6)	76 (42)
H(13′A)	241 (9)	325 (6)	1 (4)	14 (21)
H(13′B)	287 (12)	326 (9)	67 (5)	57 (36)
H(14′A)	489 (12)	375 (8)	17 (5)	46 (33)
H(14′B)	503 (10)	376 (8)	86 (5)	35 (28)
H(14′C)	475 (12)	274 (9)	53 (5)	51 (34)

and refinement data are available in the supplementary material for the 298 and 363 K determinations. In the case of the 298 K structure determination, difference Fourier synthesis indicated several elements of positional disorder, including the carbon atoms of the *n*-butyl substituent oriented perpendicular to the cyclopentadienyl ring. Final positional and isotropic thermal parameters resultant from the refinement of the 298 K data are available as supplementary material.

(21) Bolhuis, F. V. *J. Appl. Crystallogr.* **1971**, *4*, 263.
(22) "International Tables for X-Ray Crystallography"; Kynoch Press: Birmingham, England, 1962; Vol. III.
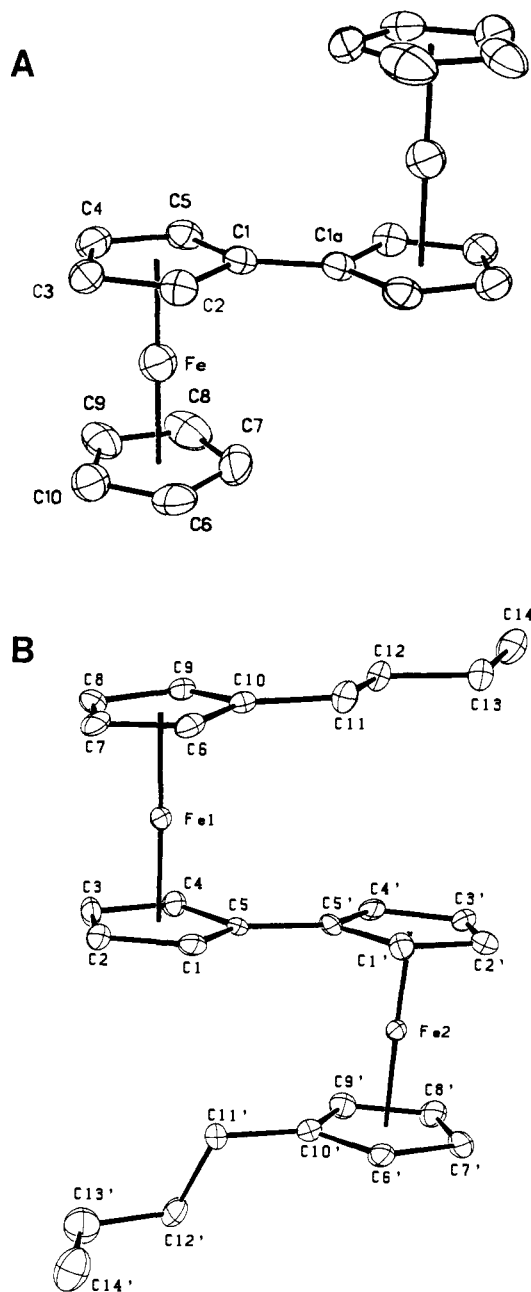(23) Stewart, R. F.; Davidson, E. R.; Simpson, W. T. *J. Chem. Phys.* **1965**, *42*, 3175.

Figure 1. ORTEP plots of biferrocenium cation in **1** (A) at 296 K and 1′,6′-di-*n*-butylbiferrocenium cation in **7** (B) at 150 K. Both are plotted with 50% probability thermal ellipsoids.

Table V. Bond Lengths (Å) and Bond Angles (deg) for Biferrocenium Triiodide

Bond Lengths			
I(1)–I(2)	2.9292 (6)	I(1)–I(2a)	2.9292 (6)
Fe(1)–C(1)	2.071 (5)	Fe(1)–C(2)	2.050 (4)
Fe(1)–C(3)	2.048 (4)	Fe(1)–C(4)	2.060 (5)
Fe(1)–C(5)	2.053 (5)	Fe(1)–C(6)	2.081 (6)
Fe(1)–C(7)	2.039 (7)	Fe(1)–C(8)	2.063 (5)
Fe(1)–C(9)	2.070 (6)	Fe(1)–C(10)	2.068 (6)
C(1)–C(2)	1.422 (6)	C(1)–C(5)	1.428 (7)
C(1)–C(1a)	1.455 (11)	C(2)–C(3)	1.402 (8)
C(3)–C(4)	1.419 (7)	C(4)–C(5)	1.418 (8)
C(6)–C(7)	1.408 (12)	C(6)–C(10)	1.387 (11)
C(7)–C(8)	1.439 (12)	C(8)–C(9)	1.400 (10)
C(9)–C(10)	1.405 (8)		

Bond Angles			
I(2)–I(1)–I(2a)	180.0	C(1)–Fe(1)–C(2)	40.4 (2)
C(1)–Fe(1)–C(3)	67.9 (2)	C(2)–Fe(1)–C(3)	40.0 (2)
C(1)–Fe(1)–C(4)	67.9 (2)	C(2)–Fe(1)–C(4)	67.6 (2)
C(3)–Fe(1)–C(4)	40.4 (2)	C(1)–Fe(1)–C(5)	40.5 (2)
C(2)–Fe(1)–C(5)	67.8 (2)	C(3)–Fe(1)–C(5)	67.9 (2)
C(4)–Fe(1)–C(5)	40.3 (2)	C(1)–Fe(1)–C(6)	125.0 (3)
C(2)–Fe(1)–C(6)	108.2 (2)	C(3)–Fe(1)–C(6)	121.3 (2)
C(4)–Fe(1)–C(6)	156.4 (3)	C(5)–Fe(1)–C(6)	161.8 (3)
C(1)–Fe(1)–C(7)	108.9 (4)	C(2)–Fe(1)–C(7)	122.3 (3)
C(3)–Fe(1)–C(7)	156.5 (3)	C(4)–Fe(1)–C(7)	162.1 (3)
C(5)–Fe(1)–C(7)	125.9 (3)	C(6)–Fe(1)–C(7)	39.9 (3)
C(1)–Fe(1)–C(8)	122.9 (2)	C(2)–Fe(1)–C(8)	158.3 (3)
C(3)–Fe(1)–C(8)	160.5 (3)	C(4)–Fe(1)–C(8)	124.6 (2)
C(5)–Fe(1)–C(8)	108.6 (2)	C(6)–Fe(1)–C(8)	68.1 (3)
C(7)–Fe(1)–C(8)	41.1 (3)	C(1)–Fe(1)–C(9)	157.8 (2)
C(2)–Fe(1)–C(9)	160.6 (2)	C(3)–Fe(1)–C(9)	124.8 (2)
C(4)–Fe(1)–C(9)	108.7 (2)	C(5)–Fe(1)–C(9)	122.6 (2)
C(6)–Fe(1)–C(9)	67.1 (3)	C(7)–Fe(1)–C(9)	67.1 (4)
C(8)–Fe(1)–C(9)	39.6 (3)	C(1)–Fe(1)–C(10)	160.7 (2)
C(2)–Fe(1)–C(10)	125.0 (2)	C(3)–Fe(1)–C(10)	108.9 (2)
C(4)–Fe(1)–C(10)	122.9 (2)	C(5)–Fe(1)–C(10)	157.7 (2)
C(6)–Fe(1)–C(10)	39.1 (3)	C(7)–Fe(1)–C(10)	65.9 (4)
C(8)–Fe(1)–C(10)	66.5 (2)	C(9)–Fe(1)–C(10)	39.7 (2)
Fe(1)–C(1)–C(2)	69.0 (3)	Fe(1)–C(1)–C(5)	69.1 (3)
C(2)–C(1)–C(5)	106.8 (5)	Fe(1)–C(1)–C(1a)	122.5 (4)
C(2)–C(1)–C(1a)	127.0 (5)	C(5)–C(1)–C(1a)	126.0 (5)
Fe(1)–C(2)–C(1)	70.6 (2)	Fe(1)–C(2)–C(3)	69.9 (2)
C(1)–C(2)–C(3)	109.0 (4)	Fe(1)–C(3)–C(2)	70.0 (2)
Fe(1)–C(3)–C(4)	70.2 (2)	C(2)–C(3)–C(4)	108.2 (4)
Fe(1)–C(4)–C(3)	69.3 (3)	Fe(1)–C(4)–C(5)	69.6 (3)
C(3)–C(4)–C(5)	107.7 (5)	Fe(1)–C(5)–C(1)	70.4 (3)
Fe(1)–C(5)–C(4)	70.1 (3)	C(1)–C(5)–C(4)	108.3 (4)
Fe(1)–C(6)–C(7)	68.4 (4)	Fe(1)–C(6)–C(10)	70.0 (3)
C(7)–C(6)–C(10)	106.1 (6)	Fe(1)–C(7)–C(6)	71.6 (4)
Fe(1)–C(7)–C(8)	70.4 (4)	C(6)–C(7)–C(8)	109.2 (8)
Fe(1)–C(8)–C(7)	68.6 (3)	Fe(1)–C(8)–C(9)	70.5 (3)
C(7)–C(8)–C(9)	106.3 (6)	Fe(1)–C(9)–C(8)	69.9 (4)
Fe(1)–C(9)–C(10)	70.1 (3)	C(8)–C(9)–C(10)	107.8 (6)
Fe(1)–C(10)–C(6)	71.0 (4)	Fe(1)–C(10)–C(9)	70.2 (4)
C(6)–C(10)–C(9)	110.6 (6)		

In the case of the 363 K structure refinement for **7**, the starting coordinates of Fe, I, and ring C atoms deduced from the 150 K refinement were employed initially. Difference Fourier synthesis indicated the presence of positional disorder in the cation and anion. The butyl group which lies perpendicular to the cyclopentadienyl ligand it is attached to shows pronounced disorder. Final positional and isotropic thermal parameters resultant from the refinement of the 363 K data are available as supplementary material.

Results and Discussion

Before the new physical data and theoretical model are described, a summary of single-crystal X-ray structural results obtained for a "chunk"-like crystal of **1** and a needle crystal of **7** are presented. These X-ray structural results will be compared with those very recently reported[24] for compound **6**.

Single-Crystal X-ray Structure of 1. The results of our crystallographic study at 300 K of **1** show that it crystallizes in the

triclinic space group $P\bar{1}$. Both the I_3^- and biferrocenium cations sit on crystallographic centers of symmetry. A perspective drawing of the biferrocenium cation is shown in Figure 1. As required by the presence of the center of symmetry, the mixed-valence cation assumes a trans conformation with the two iron ions on opposite sides of the planar fulvenide ligand. The dihedral angle between the two five-membered rings of each $Fe(\eta^5\text{-}C_5H_5)(\eta^5\text{-}C_5H_4)$ moiety is 0.3 (3)°; furthermore, the two rings are perfectly eclipsed within experimental error. A summary of bond distances and bond angles is given in Table V. Mean bond distances between the iron atom and the five carbon atoms of a given ring are 2.056 (5) and 2.064 (6) Å for the $\eta^5\text{-}C_5H_4$(fulvenide) and $\eta^5\text{-}C_5H_5$ rings, respectively. The average of these two values, i.e., 2.060 Å, lies midway between the 2.045 Å observed[25] for ferrocene and 2.075 Å observed[26] for the ferrocenium cation.

(24) Konno, M.; Hyodo, S.; Iijima, S. *Bull. Chem. Soc. Jpn.* **1982**, *55*, 2327.

(25) Seiler, P.; Dunitz, J. D. *Acta Crystallogr., Sect. B* **1979**, *35*, 1068.
(26) Mammano, N. J.; Zalkin, A.; Landers, A.; Rheingold, A. L. *Inorg. Chem.* **1977**, *16*, 297.
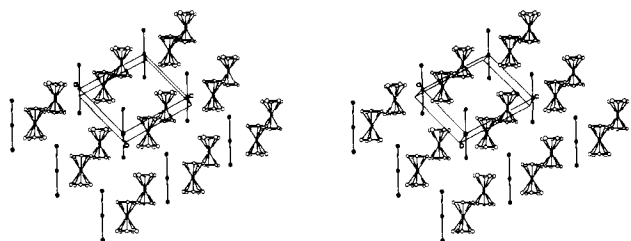
Figure 2. Stereoview of the packing arrangement of compound **1** as viewed down the *b* axis.

The triiodide anion I(1)–I(2) bond distance is 2.926 (1) Å. This corresponds well to the value of 2.920 Å reported[27] for the free I_3^- ion.

A stereoview showing the packing arrangement as viewed approximately down the *b* axis is shown in Figure 2. The structure is dominated by segregated columns of biferrocenium cations and triiodide ions parallel to the *b* axis, where each column of I_3^- anions is surrounded by four columns of the cations. The biferrocenium cations are stacked side-to-side in the columns that develop in the *b*-axis direction. The shortest interaction Fe···Fe and H···C distances in this *b*-axis direction are 5.779 (2) and 2.79 (4) Å. The shortest interanion I···I distance is 5.5981 (8) Å. As is evident from Figure 2, it is also possible to describe the packing arrangement in biferrocenium triiodide as step-like stacks of biferrocenium cations developing approximately along the ⟨011⟩ direction.

It is clear that the above crystallographic results for **1** present somewhat of a dilemma, for previous Mössbauer results[14] obtained at 300 K indicated that **1** is valence localized on the Mössbauer time scale. This means that the rate of electron transfer between the Fe^{II} and Fe^{III} sites in each cation is less than $\sim 10^7$ s^{-1}. There are several possible explanations for this apparent inconsistency. First, it is possible that there are polymorphs of **1**. The sample used for the reported Mössbauer experiments was a microcrystalline sample of **1** which forms rapidly when a benzene solution of iodine is added to a benzene solution of biferrocene. On the other hand, the crystal for the structural work was grown by slow diffusion of hexane into a CH_2Cl_2 solution of biferrocenium triiodide. We can find no evidence for the presence of polymorphs of **1**. Two different morphologies of crystals were seen in the diffusion recrystallization: "chunks" and plates, with the "chunks" being midsections of unusually large plates. The space group and unit cell parameters for the plate-like crystals were found to be the same as given in Table I for the "chunk" crystal used in the structure determination. Furthermore, an X-ray powder pattern generated from the single-crystal X-ray work agrees well with the X-ray powder pattern obtained for the microcrystalline sample of **1** (data are available as supplementary material). All three forms of **1** are the same.

A second possibility is that there is a disorder (either static or dynamic) of valence-localized biferrocenium cations throughout the crystal and a random distribution leads to a structural model with a center of symmetry positioned at each cation site. A random disorder of valence-localized biferrocenium cations should lead to thermal ellipsoids on the ring carbon atoms that are elongated perpendicular to the ring plane because it is known that Fe^{III} metallocenes have larger Fe–C bond lengths than do Fe^{II} metallocenes. However, this difference in dimensions of Fe^{II} and Fe^{III} units is small. Disorder in the cation would also require a disorder in the triiodide anion. The thermal parameters of the iodine atoms of the I_3^- anion are somewhat elongated in the direction of the I–I bond. These thermal parameters could be masking a disorder of the I_3^- anion between two positions that would accommodate the disorder in the cation. With the results of the single-crystal X-ray diffraction study it is not possible to conclude whether or not there is a disorder of valence-localized biferrocenium cations.
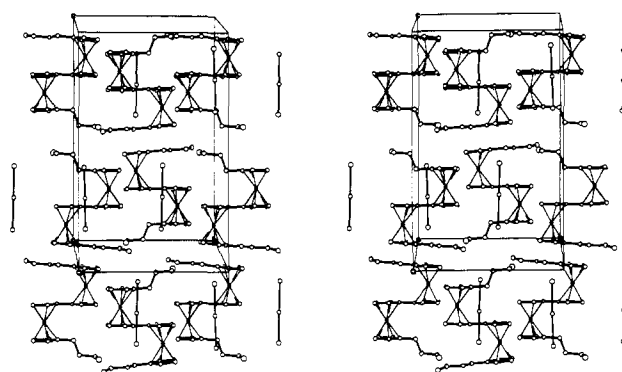
(27) Runsink, J.; Swen-Walstra, S.; Migchelsen, T. *Acta Crystallogr., Sect. B* **1972**, *28*, 1331.

Figure 3. Stereoview of the packing arrangement of compound **7** as viewed down the *a* axis.

A third possibility is that the small, presumably well-formed, crystal of **1** used for the structure determination at 296 K does have "Mössbauer-delocalized" complexes, whereas the collections of microcrystals ($\sim$15–50 mg) of **1** used in the Mössbauer experimentation do have appreciable amounts of "Mössbauer-localized" complexes. This explanation is the preferred one at this time. Data to substantiate this view are presented below.

It is interesting that compound **6** has recently been reported[24] to crystallize in $P\bar{1}$ at 298 K. Again, both the cation and anion are sitting on crystallographic centers of symmetry. In fact, the packing arrangement for **6** is essentially the same as that found for **1** (a stereoview for **6** is given in the supplementary material). There is also a cp–cp overlap between cations in the step-like stacks of cations. The neighboring cations in **6** have slipped relative to each other compared to the situation in **1**. The cp–cp distance in **6** is 3.47 (2) Å. In **6** the propylcyclopentadienyl ring was found to be rotationally disordered, with two sites in a population ratio of 3:1. In contrast to **1**, compound **6** has been reported[15] to give two Mössbauer doublets at low temperatures, which with an increase in temperature become a single doublet at 245 K. Thus, at the temperature of 298 K where the X-ray structure indicates a centrosymmetric form of the cation for **6**, there is only one doublet seen in the Mössbauer spectrum. The X-ray structure of **6** was also reported[24] at 110 K. The space group was found to be P1. There is no center of symmetry in the cation and one half looks dimensionally like a Fe^{II} and the other a Fe^{III} metallocene. It should be pointed out, however, that it is difficult to decide whether P1 or $P\bar{1}$ is the correct space group. There is no discrimination possible based on differences in extinction.

Single-Crystal X-ray Structure of 7. The single-crystal X-ray structure of a needle form of **7** was determined at three temperatures: 150, 298, and 363 K. At all three temperatures the space group is found to be $P2_1/c$. As expected, more independent reflections could be measured at 150 K than at either of the other temperatures. Consequently, the best structural results are available in the 150 K determination. A perspective drawing of the 1′,6′-di-*n*-butylbiferrocenium cation is shown in Figure 1. Table VI lists important bond distances and angles obtained from the 150 K structure determination. The 1′,6′-di-*n*-butylbiferrocenium cation assumes a trans conformation with a planar fulvenide ligand. As found for the cation in **6** at 110 K, the cation in **7** at 150 K has two dimensionally inequivalent metallocene units. One of the $Fe(\eta^5\text{-}C_5H_5)(\eta^5\text{-}C_5H_4)$ moieties in the cation has an interplane distance of 3.390 (9) Å and the other has an interplane distance of 3.313 (8) Å. In agreement with the Mössbauer data for **7** (vide infra), this suggests that the cation in **7** at 150 K is comprised of Fe^{II} and Fe^{III} units.

There are two other structural features that also indicate the cation in **7** is asymmetric at 150 K. As is evident in Figure 1, the two butyl substituents on one cation are situated differently. The carbon atom framework of one of the butyl groups runs essentially parallel to the cp ring it is attached to, whereas part of the carbon atom framework of the other butyl group runs perpendicular to the cp ring it is attached to. This asymmetry in butyl substituents points to an inequivalence in the two halves

Table VI. Bond Lengths (Å) and Bond Angles (deg) for 1',6'-Di-*n*-butylbiferrocenium Triiodide at 150 K

Bond Lengths

I(1)-I(2)	2.8977 (9)	I(2)-I(3)	2.9396 (9)	C(3)-C(4)	1.43 (1)	C(3')-C(4')	1.43 (1)
Fe(1)-C(1)	2.083 (8)	Fe(1')-C(1')	2.052 (8)	C(1)-C(5)	1.42 (1)	C(1')-C(5')	1.45 (1)
Fe(1)-C(2)	2.069 (8)	Fe(1')-C(2')	2.075 (8)	C(4)-C(5)	1.44 (1)	C(4')-C(5')	1.45 (1)
Fe(1)-C(3)	2.066 (8)	Fe(1')-C(3')	2.067 (8)	C(6)-C(7)	1.43 (1)	C(6')-C(7')	1.44 (1)
Fe(1)-C(4)	2.095 (8)	Fe(1')-C(4')	2.050 (8)	C(7)-C(8)	1.45 (1)	C(7')-C(8')	1.45 (1)
Fe(1)-C(5)	2.137 (7)	Fe(1')-C(5')	2.054 (8)	C(8)-C(9)	1.44 (1)	C(8')-C(9')	1.43 (1)
Fe(1)-C(6)	2.084 (8)	Fe(1')-C(6')	2.074 (8)	C(6)-C(10)	1.43 (1)	C(6')-C(10')	1.43 (1)
Fe(1)-C(7)	2.067 (8)	Fe(1')-C(7')	2.050 (8)	C(9)-C(10)	1.45 (1)	C(9')-C(10')	1.42 (1)
Fe(1)-C(8)	2.065 (8)	Fe(1')-C(8')	2.050 (8)	C(10)-C(11)	1.50 (1)	C(10')-C(11')	1.51 (1)
Fe(1)-C(9)	2.111 (9)	Fe(1')-C(9')	2.054 (8)	C(11)-C(12)	1.52 (1)	C(11')-C(12')	1.53 (1)
Fe(1)-C(10)	2.139 (8)	Fe(1')-C(10')	2.071 (8)	C(12)-C(13)	1.52 (1)	C(12')-C(13')	1.54 (1)
C(1)-C(2)	1.44 (1)	C(1')-C(2')	1.42 (1)	C(13)-C(14)	1.51 (1)	C(13')-C(14')	1.50 (1)
C(2)-C(3)	1.44 (1)	C(2')-C(3')	1.45 (1)			C(5)-C(5')	1.443 (10)

Bond Angles

C(1)-Fe(1)-C(2)	40.5 (3)	C(1)-Fe(1)-C(3)	67.8 (3)	Fe(1')-C(1')-C(2')	70.7 (5)	Fe(1')-C(1')-C(5')	69.5 (5)
C(1)-Fe(1)-C(5)	39.4 (3)	C(1)-Fe(1)-C(6)	108.1 (3)	Fe(1')-C(2')-C(1')	68.9 (5)	Fe(1')-C(2')-C(3')	69.2 (5)
C(1)-Fe(1)-C(8)	160.3 (3)	C(1)-Fe(1)-C(9)	157.8 (3)	Fe(1')-C(3')-C(2')	69.8 (5)	Fe(1')-C(3')-C(4')	69.1 (5)
C(2)-Fe(1)-C(3)	40.8 (3)	C(2)-Fe(1)-C(4)	68.1 (3)	Fe(1')-C(4')-C(3')	70.3 (5)	Fe(1')-C(4')-C(5')	69.4 (4)
C(2)-Fe(1)-C(6)	120.5 (3)	C(2)-Fe(1)-C(7)	105.8 (3)	Fe(1')-C(5')-C(5)	122.1 (5)	Fe(1')-C(5')-C(1')	69.3 (4)
C(2)-Fe(1)-C(9)	160.9 (3)	C(2)-Fe(1)-C(10)	156.3 (3)	C(5)-C(5')-C(1')	126.2 (7)	C(5)-C(5')-C(4')	126.0 (7)
C(3)-Fe(1)-C(5)	66.8 (3)	C(3)-Fe(1)-C(6)	156.0 (3)	Fe(1')-C(6')-C(7')	68.7 (5)	Fe(1')-C(6')-C(10')	69.7 (5)
C(3)-Fe(1)-C(8)	107.3 (3)	C(3)-Fe(1)-C(9)	125.5 (3)	Fe(1')-C(7')-C(6')	70.4 (5)	Fe(1')-C(7')-C(8')	69.2 (5)
C(4)-Fe(1)-C(5)	39.8 (3)	C(4)-Fe(1)-C(6)	162.3 (3)	Fe(1')-C(8')-C(7')	69.2 (5)	Fe(1')-C(8')-C(9')	69.8 (5)
C(4)-Fe(1)-C(8)	122.1 (3)	C(4)-Fe(1)-C(9)	110.0 (3)	Fe(1')-C(9')-C(8')	69.5 (5)	Fe(1')-C(9')-C(10')	70.5 (5)
C(5)-Fe(1)-C(6)	126.0 (3)	C(5)-Fe(1)-C(7)	160.3 (3)	Fe(1')-C(10')-C(6')	69.9 (5)	Fe(1')-C(10')-C(9')	69.2 (5)
C(5)-Fe(1)-C(9)	124.4 (3)	C(5)-Fe(1)-C(10)	111.4 (3)	C(6')-C(10')-C(9')	108.4 (7)	C(6')-C(10')-C(11')	123.6 (8)
C(6)-Fe(1)-C(8)	68.1 (3)	C(6)-Fe(1)-C(9)	67.3 (3)	C(10')-C(11')-C(12')	111.6 (7)	C(11')-C(12')-C(13')	112.3 (7)
C(7)-Fe(1)-C(8)	41.2 (3)	C(7)-Fe(1)-C(9)	68.1 (3)	Fe(1)-C(10)-C(11)	126.8 (6)	C(1)-Fe(1)-C(4)	67.4 (3)
C(8)-Fe(1)-C(9)	40.4 (3)	C(8)-Fe(1)-C(10)	67.4 (3)	C(9)-C(10)-C(11)	127.1 (8)	C(1)-Fe(1)-C(7)	123.4 (3)
C(1')-Fe(1')-C(2')	40.4 (3)	C(1')-Fe(1')-C(3')	68.8 (3)	C(12)-C(13)-C(14)	112.3 (7)	C(1)-Fe(1)-C(10)	122.8 (3)
C(1')-Fe(1')-C(5')	41.3 (3)	C(1')-Fe(1')-C(6')	108.9 (3)	C(2')-C(1')-C(5')	108.3 (7)	C(2)-Fe(1)-C(5)	67.1 (3)
C(1')-Fe(1')-C(8')	161.0 (3)	C(1')-Fe(1')-C(9')	157.6 (3)	C(1')-C(2')-C(3')	108.1 (7)	C(2)-Fe(1)-C(8)	123.3 (3)
C(2')-Fe(1')-C(3')	40.9 (3)	C(2')-Fe(1')-C(4')	68.9 (3)	C(2')-C(3')-C(4')	108.3 (7)	C(3)-Fe(1)-C(4)	40.1 (3)
C(2')-Fe(1')-C(6')	121.8 (3)	C(2')-Fe(1')-C(7')	106.7 (3)	C(3')-C(4')-C(5')	107.8 (7)	C(3)-Fe(1)-C(7)	120.8 (3)
C(2')-Fe(1')-C(9')	160.4 (3)	C(2')-Fe(1')-C(10')	157.6 (3)	Fe(1')-C(5')-C(4')	69.1 (5)	C(3)-Fe(1)-C(10)	162.4 (3)
C(3')-Fe(1')-C(5')	68.8 (3)	C(3')-Fe(1')-C(6')	156.2 (3)	C(1')-C(5')-C(4')	107.5 (6)	C(4)-Fe(1)-C(7)	156.8 (3)
C(3')-Fe(1')-C(8')	105.3 (3)	C(3')-Fe(1')-C(9')	123.2 (3)	C(7')-C(6')-C(10')	108.0 (7)	C(4)-Fe(1)-C(10)	127.1 (3)
C(4')-Fe(1')-C(5')	41.5 (3)	C(4')-Fe(1')-C(6')	162.7 (3)	C(6')-C(7')-C(8')	107.3 (7)	C(5)-Fe(1)-C(8)	158.1 (3)
C(4')-Fe(1')-C(8')	118.4 (3)	C(4')-Fe(1')-C(9')	106.3 (3)	C(7')-C(8')-C(9')	107.6 (7)	C(6)-Fe(1)-C(7)	40.2 (3)
C(5')-Fe(1')-C(6')	126.1 (3)	C(5')-Fe(1')-C(7')	162.4 (3)	C(8')-C(9')-C(10')	108.7 (7)	C(6)-Fe(1)-C(10)	39.6 (3)
C(5')-Fe(1')-C(9')	121.1 (3)	C(5')-Fe(1')-C(10')	108.9 (3)	Fe(1')-C(10')-C(11')	129.7 (6)	C(7)-Fe(1)-C(10)	67.2 (3)
C(6')-Fe(1')-C(8')	68.9 (3)	C(6')-Fe(1')-C(9')	68.2 (3)	C(9')-C(10')-C(11')	127.9 (8)	C(9)-Fe(1)-C(10)	39.8 (3)
C(7')-Fe(1')-C(8')	41.6 (3)	C(7')-Fe(1')-C(9')	69.0 (3)	C(12')-C(13')-C(14')	113.6 (8)	C(1')-Fe(1')-C(4')	69.6 (3)
C(8')-Fe(1')-C(9')	40.7 (3)	C(8')-Fe(1')-C(10')	68.4 (3)	C(2)-C(1)-C(5)	108.7 (7)	C(1')-Fe(1')-C(7')	124.3 (3)
Fe(1)-C(1)-C(2)	69.2 (4)	Fe(1)-C(1)-C(5)	72.3 (4)	C(1)-C(2)-C(3)	106.9 (7)	C(1')-Fe(1')-C(10')	123.0 (3)
Fe(1)-C(2)-C(1)	70.3 (5)	Fe(1)-C(2)-C(3)	69.5 (5)	C(2)-C(3)-C(4)	108.7 (7)	C(2')-Fe(1')-C(5')	68.6 (3)
Fe(1)-C(3)-C(2)	69.7 (5)	Fe(1)-C(3)-C(4)	71.0 (5)	C(3)-C(4)-C(5)	107.6 (7)	C(2')-Fe(1')-C(8')	123.5 (3)
Fe(1)-C(4)-C(3)	68.8 (5)	Fe(1)-C(4)-C(5)	71.7 (4)	Fe(1)-C(5)-C(5')	125.2 (5)	C(3')-Fe(1')-C(4')	40.6 (3)
Fe(1)-C(5)-C(1)	68.3 (4)	Fe(1)-C(5)-C(4)	68.5 (4)	C(4)-C(5)-C(5')	125.1 (7)	C(3')-Fe(1')-C(7')	119.5 (3)
C(1)-C(5)-C(4)	108.0 (6)	C(1)-C(5)-C(5')	126.7 (7)	C(7)-C(6)-C(10)	109.1 (7)	C(3')-Fe(1')-C(10')	160.8 (3)
Fe(1)-C(6)-C(7)	69.3 (5)	Fe(1)-C(6)-C(10)	72.2 (5)	C(6)-C(7)-C(8)	107.5 (7)	C(4')-Fe(1')-C(7')	154.3 (3)
Fe(1)-C(7)-C(6)	70.6 (5)	Fe(1)-C(7)-C(8)	69.3 (5)	C(7)-C(8)-C(9)	107.8 (7)	C(4')-Fe(1')-C(10')	125.0 (3)
Fe(1)-C(8)-C(7)	69.5 (5)	Fe(1)-C(8)-C(9)	71.5 (5)	C(8)-C(9)-C(10)	107.8 (7)	C(5')-Fe(1')-C(8')	155.2 (3)
Fe(1)-C(9)-C(8)	68.1 (5)	Fe(1)-C(9)-C(10)	71.1 (5)			C(6')-Fe(1')-C(7')	40.9 (3)
Fe(1)-C(10)-C(6)	68.1 (5)	Fe(1)-C(10)-C(9)	69.0 (5)			C(6')-Fe(1')-C(10')	40.4 (3)
C(6)-C(10)-C(9)	107.7 (7)	C(6)-C(10)-C(11)	125.2 (7)			C(7')-Fe(1')-C(10')	68.6 (3)
C(10)-C(11)-C(12)	114.1 (7)	C(11)-C(12)-C(13)	111.7 (7)			C(9')-Fe(1')-C(10')	40.4 (3)

of the cation. Furthermore, not only is the I₃⁻ ion asymmetric in this 150 K structure but it is disposed unequally relative to the two iron ions in the cation. A stereoview of the packing arrangement of **7** at 150 K is shown in Figure 3. In **7** at 150 K bond distances of I(1)-I(2) = 2.939 (1) Å and I(2)-I(3) = 2.898 (1) Å are found. There is a slight I₂·I⁻ character, where the I(1) atom probably carries more negative charge than the other terminal iodine atom I(3). In this regard it is interesting to note that the I(1) atom is closer to one iron ion, the Fe^{III} ion, than the other iron ion. It appears that it is the bulkiness of the butyl substituents that is influencing the positioning of the I₃⁻ ion. The above elements of asymmetry lead to a trapped valence state for the cation in **7** at 150 K.

A comparison of Figures 2 and 3 clearly indicates that the packing arrangement in **7** is different than what is found for **1**. The prominent feature of the crystal structure of **7** is the layer structure parallel to the *bc* plane. There is obviously no cp–cp overlap between cations in the solid-state structure of **7**. It appears that the bulky butyl substituents lead to further slippage of the cations from the step-like stacks seen for **1** and **6**. The cations in **7** have slipped so much that the intercation contact grows out of a butyl group of one cation interacting with a cp ring of a neighboring cation.

A careful analysis of the 298 K X-ray structural results for **7** shows that the cation and anion are positionally disordered along the *c* axis. (The results of the 298 and 363 K structures of **7** are only reported here in a preliminary fashion; positional and isotropic thermal parameters are included in the supplementary material.) The butyl substituents and the I₃⁻ ions appear to be positionally disordered. It was not possible to model this disorder; however, evidence for the disorder can be seen in the Debye–Waller factors for these atoms, factors which are very pronounced in the direction
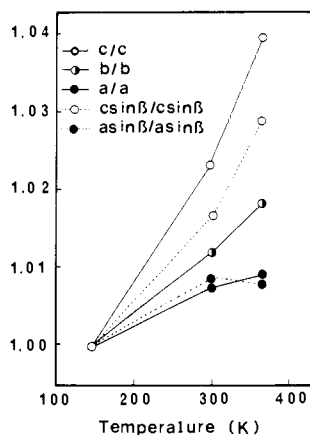
Figure 4. Unit cell parameters plotted vs. temperature for the di-*n*-butyl substituted compound 7.

Figure 5. ^{57}Fe Mössbauer spectra taken at two different temperatures for a microcrystalline sample of compound **8**.

Figure 6. ^{57}Fe Mössbauer spectra taken at various temperatures from 150 to 300 K for a diffusion-recrystallized sample of compound **8**.

of the *c* axis. Although it is, of course, difficult to conclude that these elongated thermal parameters are due to a static disorder or to dynamic motion of these atoms, it may be concluded that the molecules have an asymmetric thermal motion along the *c* axis by comparison with the results obtained from the analysis of the 150 K data. The fact that there is more thermal motion along the *c* axis at 298 K than at 150 K is also supported by the expansion of the unit cell along the *c* axis as illustrated in Figure 4 (data are given in the supplementary material). It is clear that compared to the *a* and *b* axes the *c* axis experiences a considerably greater expansion as the crystal is heated from 150 to 298 K and finally to 363 K. Reference to Figure 3 shows that it is likely the disorders in the butyl substituents and I_3^- ions are probably correlated.

When anisotropic thermal parameters were employed for the non-hydrogen atoms in the refinement of the X-ray data collected at 363 K, all of the thermal parameters became non-positive definite. A structural refinement could only be accomplished by employing fixed thermal parameters. The positions of the carbon atoms in the butyl group which lies parallel to the cp ring could be exactly determined, whereas those of the three terminal carbon atoms [C(12), C(13), and C(14)] of the other butyl group are disordered. The disorder involves the C(12)–C(13) unit librating around the C(10)–C(11) direction. This type of motion would lead to an expansion of the crystal along the *c* axis.

Physical Properties of 1',6'-Dibenzylbiferrocenium Triiodide (8). Crystalline samples of this new mixed-valence compound were prepared in three different ways. A *microcrystalline* sample is simply prepared by adding a benzene solution containing an approximately stoichiometric amount of iodine to a benzene solution of 1',6'-dibenzylbiferrocene. A more crystalline sample (X-ray work in progress) can be prepared either by slowly diffusing hexane into a CH$_2$Cl$_2$ solution containing 1',6'-dibenzylbiferrocenium triiodide or by slow evaporation of a CH$_2$Cl$_2$ solution. Microscopic examination of these crystalline forms shows that they are made up of at least two morphologies of crystals: plates and "chunks".

Two different preparations of the microcrystalline form of **8** were examined at 150 K with Mössbauer spectroscopy. Both samples gave essentially identical spectra. The 150 K spectrum for one sample is illustrated in Figure 5. The prominent features in this spectrum are two doublets, one with a quadrupole splitting (ΔE_Q) of 2.011 (6) mm/s and the other with ΔE_Q = 0.423 (7) mm/s. Both doublets have the same area as deduced by a least-squares fitting with Lorentzian line shapes. This pattern of two doublets is what is expected for a mixed-valence biferrocene which is valence trapped on the time scale of the Mössbauer technique (electron-transfer rate less than $\sim 10^7$ s^{-1}). Fitting the 150 K spectrum also clearly indicates that there is a third doublet with ΔE_Q = 1.170 (17) mm/s. This doublet is associated with a mixed-valence biferrocene with an *intra*molecular electron-transfer rate greater than $\sim 10^7$ s^{-1}. As illustrated in Figure 5, a spectrum was also run at 300 K for this same microcrystalline
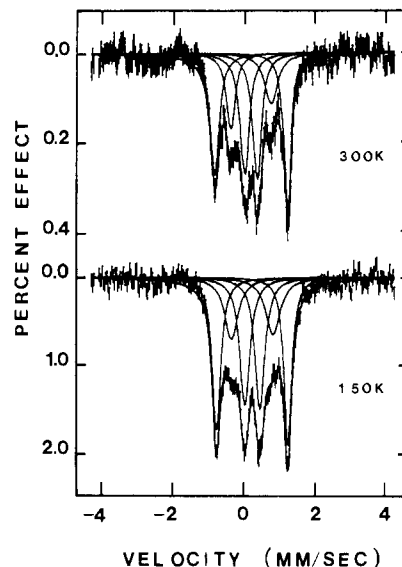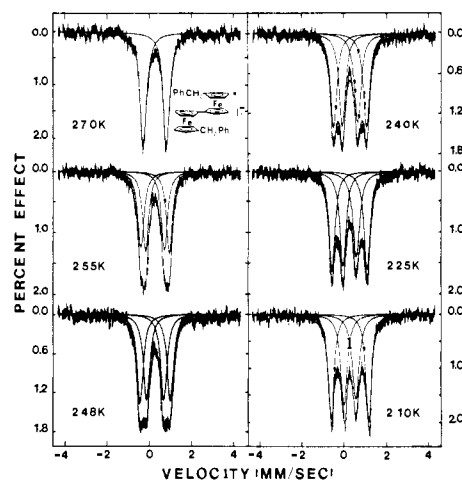
sample of **8**. The 300 K spectrum closely resembles the 150 K spectrum. The ratio of valence localized to valence delocalized species changes from 3.0:1 to 2.3:1 as the sample temperature is changed from 150 to 300 K. Unfortunately, compound **8** decomposes at elevated temperatures. Mössbauer fitting parameters are given in Table VII.

An amazing change in the appearance of the Mössbauer spectra results when a microcrystalline sample of **8** is slowly recrystallized either by diffusing hexane into a CH$_2$Cl$_2$ solution of **8** or by slow evaporation of a CH$_2$Cl$_2$ solution of **8**. Figure 6 illustrates the spectra obtained for a diffusion-recrystallized sample of **8**. The behavior is quite different from what is seen for the microcrystalline sample. At 210 K and below only two doublets can be seen, one characteristic of a Fe^{II} metallocene and the other characteristic of a Fe^{III} metallocene. Mössbauer fitting parameters are summarized in Table VII. As the temperature of this sample is increased the two doublets just move together to become a single doublet at ~ 260 K. Above this temperature there is only one *average* doublet and the intramolecular electron transfer is faster than $\sim 10^7$ s^{-1}. Two points should be emphasized: (1) the microcrystalline and diffusion recrystallized sample give the same chemical analysis (no solvent or extra iodine); and (2) there is no line broadening evident in the spectra taken at temperatures between 210 and 260 K. This same type of temperature dependence was previously seen[15] for *microcrystalline* samples of **5** and **6**. The two doublets observed for each of these compounds become one doublet at 275 and 245 K, respectively. We have collected
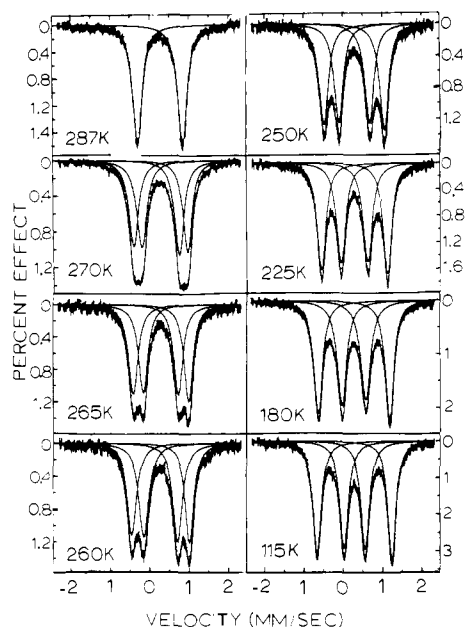
Figure 7. Variable-temperature ^{57}Fe Mössbauer spectra for a microcrystalline sample of compound **5**.
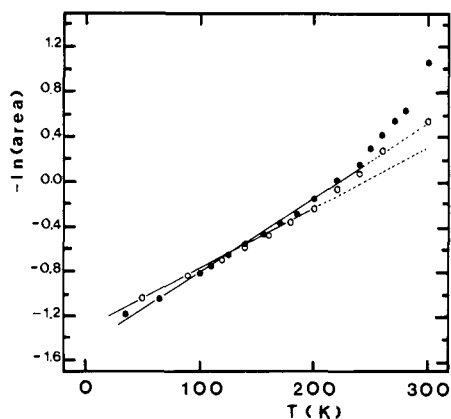

Figure 8. Plot of minus the natural logarithm of the base line normalized Mössbauer spectra area vs. temperature for the following samples: diffusion-recrystallized compound **7** (●); and microcrystalline compound **1** (○).
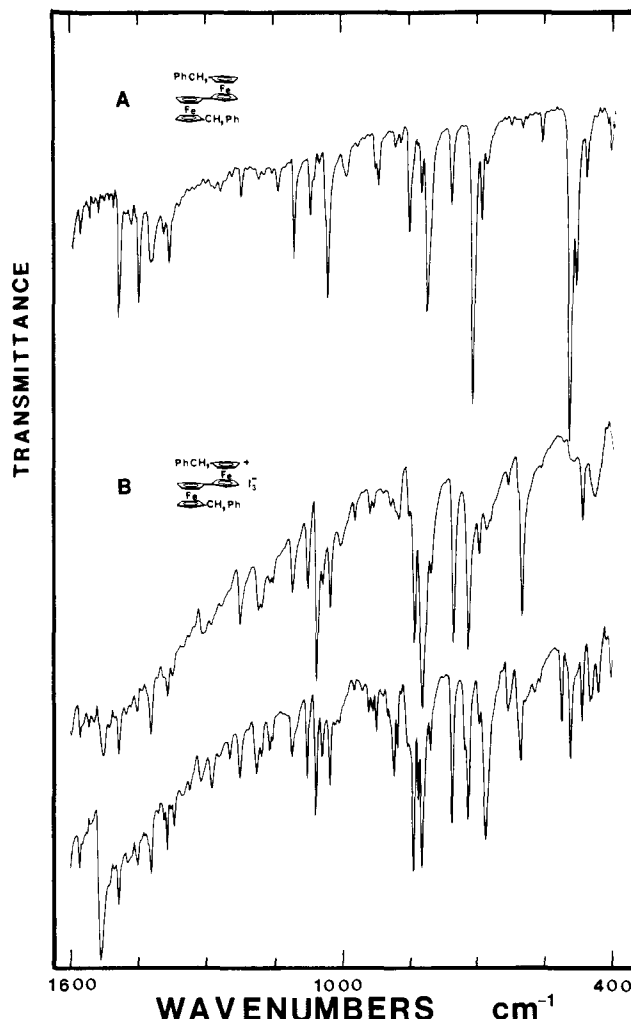

Figure 9. KBr-pellet infrared spectra of 1′,6′-dibenzylbiferrocene (A) and diffusion-recrystallized compound **8** (B) at two temperatures: 300 K spectrum is top trace in part B; 50 K spectrum is lower trace in part B.

considerably improved Mössbauer spectra for **5**. Some of our spectra are illustrated in Figure 7. There is no evidence of line broadening.

The plot of natural logarithm of the Mössbauer spectral area (background normalized) vs. temperature for a recrystallized sample of **8** is similar to that for **1** which is shown in Figure 8. In the context of a Debye model for a solid, a plot of ln (area) vs. temperature is expected[28] to give a straight line at temperatures above ∼50-100 K. That is, the recoilless fraction at a ^{57}Fe atom in the lattice reflects the Debye temperature (vibrational modes) of the solid. If the nature of the solid changes at some temperature, then there may be a change in the ln (area) vs. temperature behavior from one straight-line dependence to a different straight-line dependence. Straight-line plots of ln (area) vs. temperature have been obtained[29] from Mössbauer spectra taken in the region of 120-300 K for both ferrocenium triiodide and the valence-localized mixed-valence complex *exo,exo*-1,12-dimethyl[1.1]ferrocenophanium triiodide. For compound **8** the plot of ln (area) vs. temperature shows one straight-line behavior in

the region of ∼75 to ∼210 K. At ∼220 K there is a change to a second straight-line behavior. Compared to the behavior seen in the region of ∼75 to ∼210 K, the recoilless fraction of **8** is reduced above ∼220 K. Above ∼220 K the lattice becomes "softer". There is an increase in the availability of lattice vibrational modes for recoil of the ^{57}Fe atoms. This "break" at ∼220 K could result from a structural phase transition occurring at this temperature. This is interesting, for it is approximately at this same temperature where the electron-transfer "averaging" process begins to occur for **8** (see Figure 6) and the two doublets *begin* to move together.

A plot of -ln (area) vs. temperature taken from our new Mössbauer data on **5** also shows a "break" at approximately the same temperature. It is likely that there is also a structural phase transition present in 1′,6′-diethylbiferrocenium triiodide.

In an effort to understand the origin of the dramatic difference in 300 K Mössbauer spectra of the microcrystalline and diffusion-recrystallized forms of **8**, powder X-ray diffraction (XRD) patterns were run at 300 K for both types of samples. The powder patterns are available as supplementary material. According to the Mössbauer analysis, the microcrystalline sample examined by powder XRD was comprised of 70% localized species and 30% delocalized species. A comparison of the pattern for the microcrystalline sample with that obtained for the diffusion-recrystallized sample seems to indicate that there are two different crystalline forms present. However, it would require a determination by single-crystal X-ray diffraction techniques to establish definitively that there are two different polymorphs of **8**.

IR spectra taken at both 300 and 50 K for the two different crystalline forms of **8** also show that there is some difference.

(28) Greenwood, N. N.; Gibb, T. C. "Mössbauer Spectroscopy"; Chapman and Hall Ltd.: London, 1971.

(29) Moore, M. F.; Wilson, S. R.; Cohn, M. J.; Dong, T.-Y.; Mueller-Westerhoff, U. T.; Hendrickson, D. N. *Inorg. Chem.*, in press.

Table VII. ^{57}Fe Mössbauer Least-Squares Fitting Parameters[a]

compound	T, K	ΔE_Q, mm/s	δ, mm/s	Γ,[b] mm/s	% deloc; % loc
biferrocene[c]	78	2.34	0.52		
di-n-butylbiferrocene	140	2.394 (1)	0.527 (1)	0.278 (2), 0.264 (2)	
dibenzylbiferrocene	140	2.409 (1)	0.514 (1)	0.314 (2), 0.292 (2)	
8 (microcrystalline)	300	2.049 (8)	0.443 (4)	0.306 (17), 0.232 (12)	30; 70
		1.140 (21)	0.450 (11)	0.298 (44), 0.444 (66)	
		0.448 (9)	0.440 (5)	0.310 (17), 0.298 (16)	
	150	2.011 (6)	0.492 (3)	0.286 (12), 0.258 (12)	25; 75
		1.170 (17)	0.490 (8)	0.464 (74), 0.500 (78)	
		0.423 (7)	0.498 (4)	0.342 (13), 0.332 (12)	
8 (recrystallized)	300	1.104 (4)	0.508 (2)	0.328 (7), 0.320 (7)	
	270	1.104 (4)	0.515 (2)	0.362 (7), 0.364 (7)	
	255	1.349 (7)	0.507 (4)	0.358 (12), 0.330 (11)	
		0.892 (7)	0.501 (4)	0.340 (11), 0.348 (11)	
	250	1.429 (6)	0.514 (3)	0.346 (10), 0.358 (10)	
		0.814 (6)	0.515 (3)	0.362 (10), 0.362 (10)	
	240	1.559 (6)	0.516 (3)	0.362 (9), 0.364 (9)	
		0.733 (6)	0.513 (3)	0.366 (9), 0.382 (9)	
	225	1.666 (5)	0.511 (2)	0.336 (7), 0.342 (7)	
		0.635 (5)	0.515 (3)	0.354 (4), 0.392 (5)	
	210	1.769 (4)	0.515 (2)	0.320 (7), 0.312 (6)	
		0.557 (5)	0.516 (3)	0.370 (4), 0.394 (9)	
	180	1.891 (3)	0.514 (2)	0.296 (5), 0.298 (8)	
		0.504 (5)	0.520 (3)	0.416 (8), 0.467 (10)	
	120	1.971 (2)	0.518 (1)	0.268 (3), 0.276 (3)	
		0.479 (7)	0.517 (3)	0.560 (10), 0.630 (12)	
	80	1.985 (2)	0.508 (1)	0.276 (3), 0.274 (3)	
		0.443 (4)	0.516 (2)	0.412 (6), 0.442 (6)	
	50	2.007 (2)	0.507 (1)	0.268 (3), 0.272 (3)	
		0.422 (3)	0.516 (1)	0.358 (4), 0.362 (4)	
	30	2.046 (2)	0.515 (1)	0.274 (2), 0.270 (3)	
		0.422 (2)	0.514 (1)	0.348 (4), 0.354 (4)	
	51	2.000 (2)	0.509 (1)	0.264 (2), 0.268 (2)	
		0.411 (2)	0.520 (1)	0.346 (4), 0.346 (4)	
7 (microcrystalline)	295	1.888 (29)	0.437 (15)	0.272 (52), 0.394 (60)	76; 24
		1.240 (8)	0.475 (4)	0.444 (38), 0.516 (38)	
		0.626 (15)	0.458 (8)	0.210 (36), 0.250 (45)	
	280	1.801 (23)	0.468 (11)	0.300 (46), 0.310 (45)	63; 37
		1.180 (7)	0.473 (3)	0.410 (50), 0.462 (52)	
		0.654 (14)	0.464 (7)	0.252 (34), 0.288 (40)	
	270	1.784 (18)	0.478 (9)	0.316 (41), 0.316 (43)	54; 46
		1.192 (10)	0.480 (5)	0.476 (74), 0.520 (78)	
		0.665 (11)	0.466 (6)	0.282 (40), 0.284 (40)	
	260	1.796 (14)	0.476 (7)	0.322 (30), 0.314 (28)	38; 62
		1.167 (12)	0.477 (6)	0.466 (91), 0.486 (94)	
		0.664 (8)	0.467 (4)	0.288 (22), 0.300 (24)	
	250	1.793 (10)	0.487 (5)	0.324 (20), 0.314 (10)	21; 79
		1.153 (18)	0.491 (9)	0.414 (59), 0.474 (63)	
		0.666 (7)	0.476 (3)	0.322 (12), 0.310 (16)	
	240	1.816 (8)	0.489 (4)	0.310 (12), 0.300 (7)	17; 83
		1.156 (18)	0.470 (9)	0.370 (50), 0.410 (54)	
		0.644 (6)	0.482 (3)	0.296 (10), 0.308 (10)	
	210	1.863 (3)	0.496 (1)	0.322 (4), 0.294 (4)	0; 100
		0.650 (3)	0.490 (1)	0.323 (4), 0.334 (4)	
	180	1.895 (2)	0.407 (1)	0.310 (4), 0.294 (4)	0; 100
		0.627 (2)	0.402 (1)	0.320 (4), 0.334 (4)	
	150	1.919 (2)	0.511 (1)	0.314 (3), 0.258 (3)	0; 100
		0.623 (2)	0.511 (1)	0.340 (4), 0.346 (4)	
	120	1.932 (2)	0.519 (1)	0.314 (3), 0.288 (3)	0; 100
		0.611 (2)	0.519 (1)	0.334 (3), 0.340 (4)	
7 (recrystallized)	300	1.202 (5)	0.491 (2)	0.372 (8), 0.394 (8)	
	280	1.197 (5)	0.521 (2)	0.402 (8), 0.420 (8)	
	270	1.422 (8)	0.529 (4)	0.332 (14), 0.330 (14)	
		0.964 (8)	0.519 (4)	0.332 (13), 0.348 (14)	
	260	1.520 (7)	0.519 (4)	0.384 (12), 0.356 (10)	
		0.907 (7)	0.499 (3)	0.362 (10), 0.356 (10)	
	250	1.604 (7)	0.504 (3)	0.384 (11), 0.366 (10)	
		0.839 (6)	0.491 (3)	0.352 (9), 0.352 (9)	
	240	1.727 (6)	0.507 (3)	0.368 (12), 0.330 (12)	
		0.755 (6)	0.492 (3)	0.338 (10), 0.320 (10)	
	220	1.821 (5)	0.506 (2)	0.304 (9), 0.282 (8)	
		0.699 (5)	0.495 (2)	0.336 (9), 0.302 (8)	
	200	1.848 (5)	0.508 (2)	0.308 (10), 0.274 (8)	
		0.676 (5)	0.498 (2)	0.312 (8), 0.292 (8)	
	185	1.900 (5)	0.521 (2)	0.312 (9), 0.294 (8)	
		0.667 (4)	0.500 (2)	0.312 (8), 0.304 (8)	
	170	1.899 (5)	0.514 (2)	0.352 (10), 0.294 (8)	
		0.687 (5)	0.508 (2)	0.318 (8), 0.314 (8)	

Table VII (Continued)

compound	T, K	ΔE_Q, mm/s	δ, mm/s	Γ,[b] mm/s	% deloc; % loc
	155	1.909 (4)	0.524 (2)	0.332 (8), 0.298 (7)	
		0.699 (4)	0.517 (2)	0.332 (8), 0.338 (8)	
	140	1.900 (4)	0.521 (2)	0.362 (8), 0.304 (7)	
		0.699 (4)	0.517 (2)	0.342 (7), 0.340 (7)	
	125	1.934 (4)	0.527 (2)	0.348 (7), 0.310 (6)	
		0.698 (4)	0.525 (2)	0.332 (6), 0.332 (7)	
	110	1.920 (4)	0.528 (2)	0.350 (8), 0.308 (7)	
		0.682 (4)	0.525 (2)	0.334 (7), 0.330 (7)	
	65	1.930 (3)	0.522 (2)	0.344 (6), 0.302 (5)	
		0.669 (3)	0.528 (2)	0.314 (5), 0.314 (5)	
	33	1.924 (3)	0.524 (1)	0.332 (5), 0.294 (5)	
		0.658 (3)	0.529 (1)	0.316 (5), 0.304 (5)	
	5	1.924 (3)	0.526 (1)	0.328 (4), 0.290 (4)	
		0.657 (3)	0.533 (1)	0.324 (4), 0.310 (4)	
1 (microcrystalline)[d]	302	1.908 (6)	0.486 (3)	0.276 (12), 0.260 (11)	12; 88
		1.110 (176)	0.487 (88)	0.346 (96), 0.938 (224)	
		0.386 (6)	0.487 (3)	0.292 (12), 0.282 (12)	
	318	2.002 (6)	0.582 (3)	0.304 (12), 0.298 (12)	22; 78
		0.997 (29)	0.475 (14)	0.404 (62), 0.658 (92)	
		0.420 (6)	0.517 (3)	0.302 (10), 0.316 (13)	
	325	1.957 (10)	0.504 (5)	0.350 (18), 0.360 (20)	28; 72
		1.101 (21)	0.487 (10)	0.396 (62), 0.608 (76)	
		0.462 (8)	0.511 (4)	0.324 (14), 0.308 (15)	
	335	1.794 (36)	0.519 (18)	0.420 (42), 0.410 (52)	40; 60
		1.106 (14)	0.497 (7)	0.402 (90), 0.452 (100)	
		0.529 (30)	0.501 (15)	0.410 (37), 0.402 (38)	
	347	1.130 (8)	0.505 (4)	0.566 (14), 0.630 (16)	100; 0

[a] The estimated standard deviations in the least-significant figures are given in parentheses. [b] Full width at half-height taken from the least-squares fitting program. The width for the line at more negative velocity is listed first for each doublet. [c] G. K. Wertheim and R. H. Herber, *J. Chem. Phys.* **1963**, *38*, 2106. [d] The parameters for **1** were obtained by fitting spectra run on a ±4 mm/s velocity range.
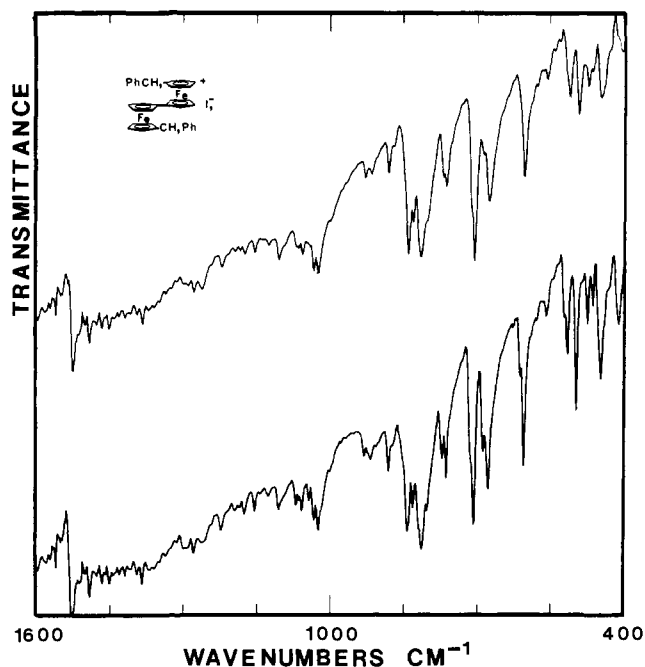

Figure 10. KBr-pellet infrared spectra of a microcrystalline sample of compound **8** at two tempertures: 300 K (top); 50 K (bottom).

Figures 9 and 10 show the KBr-pellet FTIR spectra for unoxidized 1′,6′-dibenzyliferrocene and the two crystalline forms of **8**. The most obvious difference between the spectra in Figures 9 and 10 is that there is a temperature dependence in the case of the diffusion-recrystallized sample (Figure 9), whereas there is little temperature dependence evident in the spectra for the microcrystalline sample. In the former case bands at 1525 and 690 cm⁻¹ grow in intensity compared to other peaks as the temperature is decreased. It can be seen that the enhancement in intensity in the 690-cm⁻¹ band is quite pronounced. The bands seen for the microcrystalline sample (Figure 10) are broader and in the 650–800 cm⁻¹ region are shifted compared to bands seen for the other sample.

Previous work[30] on mixed-valence biferrocenes has indicated that the C–H bending bands in the infrared spectrum can be employed to tell whether a given mixed-valence biferrocene is delocalized or not. This band is seen at 815 cm⁻¹ for ferrocene and 851 cm⁻¹ for ferrocenium triiodide.[31] There seems to be no question that the bis(fulvalene)diiron cation in various salts has a delocalized ground state.[32] The direct and indirect Fe–Fe electronic interactions have eliminated any barrier in the ground state. A single C–H bending band is seen[30] at 824 cm⁻¹ for the I_5^- salt of the bis(fulvalene)diiron cation. Mixed-valence biferrocenes that have a non-negligible potential-energy barrier for electron transfer should exhibit one C–H bending band for the Fe^{II} moiety and one for the Fe^{III} moiety. This has been established for several mixed-valence biferrocenes.[30,33] 1′,6′-Dibenzylbiferrocene (Figure 9) does show one strong C–H bending band at 812 cm⁻¹. Two bands at 820 and 839 cm⁻¹ are seen at 300 K and essentially two bands at 818 and 841 cm⁻¹ are seen at 50 K for diffusion-recrystallized **8**. The microcrystalline sample of **8** also has these same two bands. This indicates that the *intra*molecular electron transfer is slower than the inverse of the IR time scale.

Physical Properties of Biferrocenium Triiodide (1). With the single-crystal X-ray structural results in hand it was important to take a careful look at the physical data for this key compound. We reconfirmed that a microcrystalline sample of **1**, formed by adding a benzene solution of iodine to a benzene solution of biferrocene, does exhibit essentially two doublets in its 300 K Mössbauer spectrum. However, it was curious to find that a plot of ln (area) vs. temperature for such a microcrystalline sample showed a "break" in a straight-line dependence at 215 K (see Figure 8). Why is there such a "break" for a compound that is valence-localized on the Mössbauer time scale? Part of the answer to this question is evident in Figure 11 which illustrates Mössbauer spectra taken for a microcrystalline sample of **1** in the temperature range of 302–357 K. A third doublet with ΔE_Q = 1.08 mm/s

(30) Kramer, J. A.; Hendrickson, D. N. *Inorg. Chem.* **1980**, *19*, 3330.
(31) Duggan, D. M.; Hendrickson, D. N. *Inorg. Chem.* **1975**, *14*, 955 and references therein.
(32) Hillman, M.; Kvick, A. *Organometallics* **1983**, *2*, 1780.
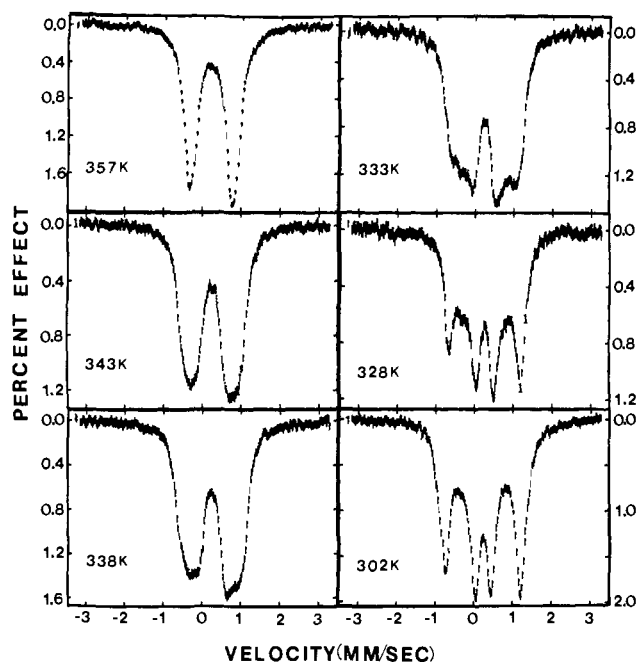(33) Kramer, J. A.; Herbstein, F. H.; Hendrickson, D. N. *J. Am. Chem. Soc.* **1980**, *102*, 2293.

8006   *J. Am. Chem. Soc., Vol. 107, No. 26, 1985*

Dong et al.

Figure 11. Variable-temperature ^{57}Fe Mössbauer spectra of a microcrystalline sample of compound **1** in the range of 300 to 357 K.

Figure 12. Variable-temperature ^{57}Fe Mössbauer spectra of a diffusion-recrystallized sample of compound **7**.

can be seen at 327 K. Fitting parameters are given in Table VII. These parameters were obtained by fitting ±4 mm/s velocity range spectra, which due to their larger velocity range give a better assessment of the base line. In fact, close examination of the 302 K spectrum shows that there is some of this third doublet present. Further increase in the temperature of the sample leads to an increase in the relative intensity of this third doublet at the expense of the Fe^{II} and Fe^{III} doublets. At 357 K only this third doublet is present. When the sample is then cooled back to 300 K the Mössbauer spectrum that is obtained is essentially identical with the one originally obtained at 300 K. Furthermore, in independent experiments (prolonged heating followed by chemical analysis) it was shown that compound **1** is thermally stable at these elevated temperatures and does not lose iodine. The characteristics of the third doublet indicate that it results from a valence-delocalized form of **1**.

At this time it is only possible to speculate about why the 300 K Mössbauer spectrum for a microcrystalline sample of **1** is basically that of a valence-localized species, whereas the X-ray structure of a "chunk" crystal of **1** indicates a centrosymmetric cation. Several different samples of **1** were investigated with Mössbauer spectroscopy. In the case of certain diffusion-recrystallized samples of **1**, we did see an appreciable increase in the amount of the third doublet in the 300 K spectrum. In fact, for one sample the 300 K spectrum showed essentially equal amounts of the delocalized and localized complexes. All of the facts taken together suggest that there is a phase transition present in **1** and that it is the level of crystallinity in a given sample of mixed-valence salt that determines the temperature evolution of the phase transition. Poorly crystalline samples tend to have a higher concentration of defect structure and this will affect the temperature evolution of the phase transition (vide infra).

Direct evidence for the presence of a phase transition associated with the temperature dependence seen in the Mössbauer spectrum for **1** was obtained by differential scanning calorimetry measurements carried out in the range of $\sim$303 to $\sim$363 K. A relatively sharp peak characterized by ΔS = 1.1 J/(mol·deg) was seen at $\sim$335 K for a microcrystalline sample of **1** that shows essentially only a localized (i.e., two doublets) pattern in the 300 K Mössbauer spectrum. Samples of **1** which show appreciable amounts of a third doublet for a valence-delocalized species in their 300 K Mössbauer spectrum give a broad DSC peak which occurs at temperatures lower than $\sim$335 K. Furthermore, the one sample that showed the maximum amount ($\sim$40–50%) of delocalized species either apparently had such a broad peak that
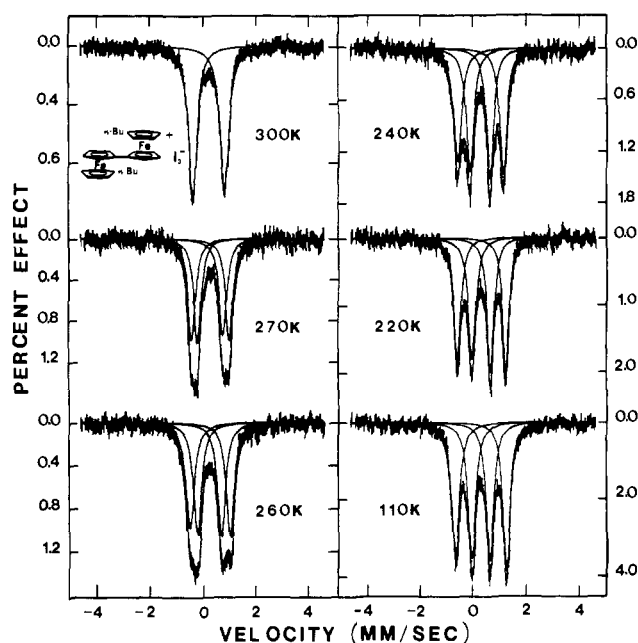
it could not be seen or the peak was shifted below $\sim$303 K.

Physical Properties of 1′,6′-Di-n-butylbiferrocenium Triiodide (7). Several of the unusual observations that have been made for **8** have also been seen for the other new mixed-valence compound reported in this paper, compound **7**. Microcrystalline samples of **7** obtained upon addition of a benzene solution of I$_2$ to a benzene solution of dibutylbiferrocene give Mössbauer spectra with both localized (two doublets) and delocalized (one average doublet) spectra superimposed. The same observation is made for a crystalline sample of **7** grown by slow evaporation of a CH$_2$Cl$_2$ solution. With different samples the ratio of localized to delocalized spectra has been seen to vary from 3:1 to 1:3 at 300 K. Crystalline samples obtained by diffusion of hexane into a CH$_2$Cl$_2$ solution of **7** give Mössbauer spectra at 300 K that show *only a single average doublet*. In Figure 12 are shown variable-temperature Mössbauer spectra obtained for diffusion-recrystallized **7**. As with the crystalline samples of **5**, **6**, and **8**, two doublets are seen to move together as the sample temperature is increased, finally to become a single average doublet at $\sim$275 K for **7**. In the plot of -ln (area) vs. temperature taken from these Mössbauer data there is a "break" in the data at $\sim$240 K, where there is a change from one straight line dependence to another.

Powder XRD patterns were run at 300 K for both a diffusion-recrystallized sample of **7** and a microcrystalline sample of **7** that the Mössbauer indicated had a 1:3 localized:delocalized composition (figure available as supplementary material). In contrast to the case of **8**, the two XRD patterns look similar. With measurements on a block crystal of **7** we have found that it has the same space group and unit cell parameters as found for the needle crystals used in the structure determination.

Variable-temperature IR spectra were also run for KBr pellets of the two types of samples of **7**. Data for the diffusion-recrystallized sample are given in Figure 13, together with a spectrum for 1′,6′-di-n-butylbiferrocene. As the sample of **7** is cooled from 300 to 50 K, a band at 1520 cm^{-1} and two bands at 680 and 690 cm^{-1} grow in intensity. The 812-cm^{-1} band observed for the unoxidized biferrocene is assignable as the C–H bending vibration of the cyclopentadienyl groups. Relatively intense bands at 820 and 839 cm^{-1} are seen for the oxidized compound **7**. If the band at 839 cm^{-1} can be assigned to a C–H bending mode of the Fe^{III} moiety, then **7** is localized on the IR time scale. The microcrystalline sample of **7** shows similar temperature dependencies as indicated in Figure 13. The spectrum for the microcrystalline form of **7** exhibits more comparable intensities in the 820- and 840-cm^{-1} bands than seen in the spectra of Figure 13.
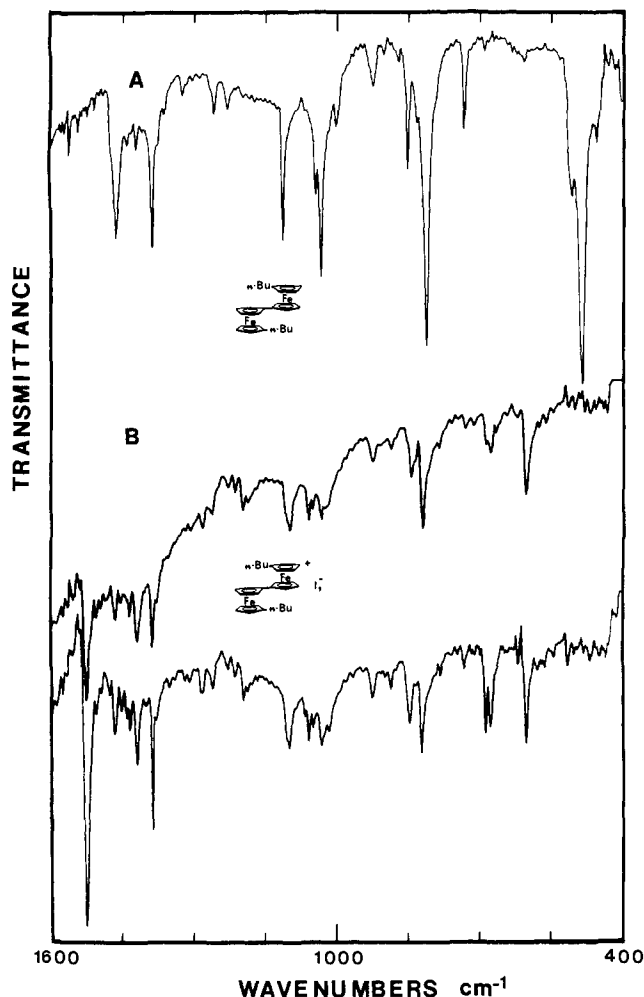
Figure 13. KBr-pellet infrared spectra of 1',6'-di-*n*-butylbiferrocene (A) and diffusion-recrystallized compound 7 (B) at two temperatures: 300 K spectrum is top trace in part B; 50 K spectrum is lower trace in part B.

Valence-Detrapping Modes in the Solid State. It is known that the mixed-valence cations in **1**, **2**, **4**, **5**, **6**, and **7** have the same trans conformation where the two iron ions are on opposite sides of a planar fulvenide ligand. It is also very likely that this is also the case for the cations in **3** and **8**. The magnitude of the electronic interaction of the d manifolds on the two iron ions, an interaction which is propagated by the fulvenide ligand, is probably not very different from one cation to another in the series **1** to **8**. Furthermore, the vibronic coupling in the PKS model[34] is also probably not changing very much throughout the series. We would suggest that it is the nature of the environment about each cation in these solids that determines whether or not *intra*molecular electron transfer occurs. The temperature dependence observed in the Mössbauer spectra for **1**, **5**, **6**, **7**, and **8** results from a phase transition in the solid state. The presence of an order–disorder phase transition which affects the *intra*molecular electron transfer in trinuclear, oxo-centered mixed-valence iron acetate complexes has already been established by variable-temperature X-ray structural[35] and heat-capacity[36] studies. Heat-capacity measurements on **1** are in progress.[37] In a recent article[38] we have

commented on the influence of the solid-state environment on the rate of *intra*molecular electron transfer in mixed-valence complexes.

The mixed-valence cation in each of the compounds **1–8** serves as a very sensitive probe of the microscopic structure of the solid state. These mixed-valence cations are one type of an electronically labile complex. They are electronically labile in the sense that in the absence of vibronic coupling there are two *energetically degenerate* electronic states of such a binuclear mixed-valence complex. This electronic degeneracy is, of course, removed by an interaction of the vibrational coordinates of the cation with the electronic coordinates (i.e., vibronic coupling). Thus, relatively minor perturbations of a mixed-valence biferrocene cation caused by interactions with neighboring cations and anions in the solid state can have pronounced effects on the electronic structure and therefore rate of *intra*molecular electron transfer.[38]

In the solid state probably the single most important factor controlling *intra*molecular electron transfer in a *symmetric*, binuclear, mixed-valence cation experiencing weak or moderate electronic coupling between the two metal centers is the positioning of the anion. If the positions of the mixed-valence biferrocenium cation and I_3^- anion are fixed and if one of the negative-charge-carrying terminal atoms of the I_3^- anion is situated closer to one iron ion of a given cation, then this iron ion will have a strong tendency to be the Fe^{III} ion. It is our suggestion that the temperature dependence observed in the Mössbauer spectra for good crystalline samples of **5**, **6**, **7**, and **8** results from a phase transition involving motion of the I_3^- anion and perhaps the substituents on the cation. At low temperature the I_3^- ion and biferrocenium cation are fixed in position. As the sample temperature is increased the phase-transition temperature is reached and each I_3^- ion begins to move between two or more positions in the lattice. This transformation could well lead to a dramatic increase in the rate of *intra*molecular electron transfer. There are actually two possibilities for the movement of the I_3^- anions. As stated above, it is possible that the I_3^- anions move as a unit in the solid. However, it is more probable that the I_3^- anions are interconverting between two configurations, one which can be described in a limiting form as $I_A^-\cdots I_B\!-\!I_C$ and the other one as $I_A\!-\!I_B\cdots I_C^-$. That is, in each configuration one I–I bond is shorter than the other one in each I_3^- anion. The thermal barrier for an I_3^- interconverting between two asymmetric configurations has been estimated[39] to be ~ 250 cm^{-1}.

If the phase transition is cooperative, then this could explain why some of the physical properties of these mixed-valence biferrocenium triiodides depend on the history of the sample. For example, diffusion-recrystallized **8** gives one average doublet in its Mössbauer spectrum at 300 K, whereas the microcrystalline sample gives two doublets at 300 K. In the case of the diffusion-recrystallized sample, the phase transition develops readily because the crystallinity is good. In the case of the microcrystalline sample there could be a considerably higher concentration of defects in a given crystal. For a cooperative phase transition, domains of a minority phase nucleate and grow in the presence of the majority phase. At low temperature the majority phase in a crystal of some mixed-valence biferrocenium triiodide would have the valence-localized form of the cation. As the temperature is increased small homogeneous regions of the valence-delocalized cations nucleate and then grow in size with increasing temperature to become eventually the majority phase. Defects in a crystal may come in the form of vacancies, isolated impurities, dislocations, grain boundaries, or surface imperfections. It is known that a high defect concentration in a crystallite can make a cooperative phase transition very gradual. The microcrystalline form of **8** could have such a high concentration of defects that the phase transition is not seen until temperatures above ~ 300 K.

It is also necessary to discuss why there is no line broadening seen in the variable-temperature Mössbauer spectra of crystalline

(34) Wong, K. Y.; Schatz, P. N. *Prog. Inorg. Chem.* **1981**, *28*, 369 and references therein.

(35) (a) Oh, S. M.; Hendrickson, D. N.; Hassett, K. L.; Davis, R. E. *J. Am. Chem. Soc.* **1984**, *106*, 7984. (b) Oh, S. M.; Hendrickson, D. N.; Hassett, K. L.; Davis, R. E. *J. Am. Chem. Soc.*, in press.

(36) (a) Oh, S. M.; Kambara, T.; Hendrickson, D. N.; Sorai, M.; Kaji, K.; Woehler, S. E.; Wittebort, R. J. *J. Am. Chem. Soc.* **1985**, *107*, 5540. (b) Sorai, M.; Kaji, K.; Hendrickson, D. N.; Oh, S. M. *J. Am. Chem. Soc.*, in press.

(37) Sorai, M.; Dong, T.-Y.; Hendrickson, D. N., unpublished results.

(38) Hendrickson, D. N.; Oh, S. M.; Dong, T.-Y.; Kambara, T.; Cohn, M. J.; Moore, M. F. *Comments Inorg. Chem.*, in press.

(39) Brown, R. D.; Nunn, E. K. *Aust. J. Chem.* **1966**, *19*, 1567.

samples of **5, 6, 7,** and **8.** As the sample temperature is increased the two doublets just move together to become a single average doublet. The line widths of the components of the "Fe^{II}" and "Fe^{III}" doublets do *not* increase at intermediate temperatures. If each binuclear mixed-valence complex had an unchanging potential energy barrier, then an increase in the thermal energy would increase the rate of electron transfer. Eventually in some temperature region the rate of electron transfer would go through the range 10^6–10^8 s^{-1} that can be sensed by the Mössbauer technique. The line shapes of the Mössbauer spectra should be affected (broadened).

If the suggestion about the presence of a phase transition is correct, then it is understandable why no line broadening is being seen in the Mössbauer spectra. In effect, we are *not* directly seeing the intramolecular electron transfer. It is likely that the averaging that is being seen is the result of lattice dynamics in the solid state. The lattice librations, i.e., phonons, that are operative in the process wherein the I$_3^-$ and substituent atoms become dynamic are occurring at a frequency greatly in excess of 10^8 s^{-1}. These phonon modes are the valence-detrapping modes in the solid state. When a given mixed-valence cation achieves the situation where the I$_3^-$ anion is disposed symmetrically relative to both iron ions in the cation, intramolecular electron transfer occurs at a rate that is faster than can be gauged by the Mössbauer technique.

Recently the influence of solid-state effects on the properties of spin-crossover complexes has been recognized.[40] Spin-crossover complexes have been identified that undergo relatively sudden transformations in the solid state, where within a few degrees the whole sample converts from high to low spin. A first-order phase transition is present in these sudden spin-crossover complexes. It is likely that long-range *inter*molecular interactions (hydrogen bonding indicated in certain cases) lead to the cooperativity that is seen for the phase transitions in these complexes. At tem-

peratures below the phase-transition temperature, the long-range interaction gives an ordered state. Above the transition temperature thermal energy disrupts the long-range interaction. There is still much to be learned about the microscopic nature of these sudden spin-crossover complexes. The detailed nature of the more abundant gradual spin-crossover complex is even less well-known. The question of how the solid-state structure and dynamics impact on the rate of the spin-crossover transformation for a particular complex is just beginning to be investigated.[41] As with mixed-valence complexes, these spin-crossover complexes can be probes of the dynamical nature of the solid state.

In solution the environment about the mixed-valence complex also influences the rate of *intra*molecular electron transfer. For such a cationic complex with weak or moderate electronic coupling between the metal centers, if there is ion pairing present, the anion will have to either be disposed equally relative to the metal centers or have to move rapidly so that it does not limit the rate of *intra*molecular electron transfer. The solvent structure about an uncharged complex such as one of the trinuclear oxo-centered iron acetate complexes will have to adjust rapidly as well in order not to limit the rate of electron transfer in the Fe$_3$O triangle.

Supplementary Material Available: Structure factors and thermal parameters for the structural analysis of compound **1** at 296 K and for compound **7** at 150 K; structure factors for compound **7** at 298 K; positional and isotropic thermal parameters for the structure determination of **7** at 298 and 363 K; figures showing the room-temperature powder X-ray diffraction data for **7** and **8** (56 pages). Ordering information is given on any current masthead page.

(40) (a) Gütlich, P. *Struct. Bonding (Berlin)* **1981,** *44,* 83 and references therein. (b) König, E.; Ritter, G.; Kulshreshtha, S. K. *Chem. Rev.* **1985,** *85,* 219–234.

(41) (a) Federer, W. D.; Hendrickson, D. N. *Inorg. Chem.* **1984,** *23,* 3861. (b) Federer, W. D.; Hendrickson, D. N. *Ibid.* **1984,** *23,* 3870. (c) Rao, C. N. R. *Intl. Rev. Phys. Chem.* **1985,** *4,* 19–38.